QUANTIFYING PATTERNS OF STREAMFLOW PEAKS OVER THE SOUTHEASTERN UNITED STATES USING A LONG-TERM RETROSPECTIVE DATASET

Raczyński K.[1], Dyer J.[1,2]

[1] Northern Gulf Institute, Mississippi State University, 2 Research Blvd, Starkville, MS 39759, chrisr@ngi.msstate.edu

[2] Department of Geosciences, Mississippi State University, 200A Hilbun Hall, Mississippi State, MS 39762, jamie.dyer@msstate.edu

Abstract:

Utilizing simulated daily flow values for 61,948 stream nodes from the National Water Model (NWM) v.2.1 retrospective dataset, which covers the period 1979–2020, streamflow peaks (SFP) were determined using an objective threshold method based on the Fisher-Jenks breakpoint algorithm. This approach provides estimates of low probability, high in-channel water level conditions. Strong spatial relations in temporal streamflow peak distribution were observed, with four main spatial clusters covering: (1) the central parts of Mississippi to South Carolina; (2) the south and north parts of Mississippi to South Carolina; (3) Florida, the Gulf Coast, and parts of North Carolina and Virginia; and (4) the Atlantic Coast and parts of the Gulf Coast. The first area is characterized by high multiannual SFP occurrence with long total durations, high contribution to total discharge, and occurrence throughout the year with peaks in February and March. Increasing annual peak trends are present locally. The second area is characterized by similar parameters with increased flash flooding potential. In the third area, lower occurrence and share in total discharge are observed, with two peaks of occurrence in the September-October and March periods. In the fourth region, the lowest occurrences and shortest durations are present, along with strong seasonality manifested in September-October occurrences that constitute over 80% of all SFP volumes. Decreasing trends in maximal monthly flows for the June-October period are also observed here. The results provide valuable regionalized information about historical high flow characteristics across the Southeast US, which can be used as a basis for improved long-term flood prediction based on seasonality models and constitute a baseline for defining regional changes in high flow frequency and distribution.

Keywords:

streamflow peak, flood, trend, seasonality, national water model, southeastern united states

1. Introduction

According to the National Weather Service (NWS) Annual Flood Loss Reports, the costs of flood damage in the United States (US) over the last ten years (2012-2021) reached almost $90 billion, with thousands of lives lost and hundreds of thousands of people affected. This makes flooding the most devastating and costly category of environmental disaster in the US. Looking into the future, climate change is shown to not only affect the distribution of floods, but also contribute to changes in flood magnitude, timing, and duration (Li et al., 2022a; b). Furthermore, due to climatic change it is projected that global sea levels will increase by 11–180 cm by 2100, which will increase flood losses globally between $14 and $27 trillion per year (Jevrejeva et al., 2018).

Increases in flood vulnerability are highly dependent on human factors, such as increases in urbanization or population growth, which leads to substantial variability in both flood drivers and impacts (Tramblay et al., 2019). Population within the US has increased by 10% between 2000 and 2010, resulting in a 13.6% increase in housing units and 10.7% increase in impervious surfaces, which exceeded prior estimates (Vogler & Vukomanovic, 2021). These changes further affect flood vulnerability due to increasing precipitation that translates to higher runoff, especially over urbanized areas (Niyogi et al., 2017).

Flood generation processes across the continental US (CONUS) vary spatially, with precipitation as the main driver followed by local-scale watershed attributes (Kundzewicz et al., 2019; Li et al., 2022a; Saharia et al., 2017a). In terms of precipitation, flood drivers can be divided into groups: large-scale frontal storms, monsoons, convective storms, snowmelt, and rain-on-snow (Huang et al., 2022). Meteorological factors and climate change are of the greatest importance in driving flood events through changes in precipitation characteristics, and it is projected that the frequency and spatial extent of extreme rainfall will increase in the future across the southeastern US (Cigler, 2017; Gangrade et al., 2018). This could affect the seasonality of floods and contribute to a decrease in the predictability of events (Li et al., 2022a). Building on this, due to human factors such as urbanization and population growth, flood vulnerability will increase (Mogollón et al., 2016; Tramblay et al., 2019) and floods themselves will become flashier (Li et al., 2022b). This in turn will lower the effectiveness of prediction models, that even now have low accuracy over the southeastern US due to human-induced changes to the landscape and the associated complex atmospheric drivers of flooding (Do et al., 2020). As a result, recognition of flood

characteristics, seasonality, and tendencies is crucial for better understanding of regional flood mechanisms and for adjusting flood infrastructure and models accordingly.

Although meteorological factors are critical in defining the occurrence and characteristics of floods, other factors such as soil moisture, reservoir storage, land use/land cover, and topography play important roles in the generation and evolution of flooding events (Gangrade et al., 2018; Mogollón et al., 2016). In terms of general temporal patterns, strong seasonality of flooding is observed across the United States as a result of climate and surface conditions (Villarini, 2016); therefore, understanding these underlying causes and the associated regional variability is crucial for better flood management (Ye et al., 2017). For example, a leading driver for extreme regional flooding over the southeastern and eastern US in the summer and early fall are landfalling tropical cyclones (Villarini & Smith, 2010), while for the northeastern US the occurrence of floods is often related to convective rainfall fed by tropical moisture advected from the Atlantic Ocean or Gulf of Mexico (Lu & Lall, 2016; Nakamura et al., 2013). For the southeastern US in the winter and spring, flood occurrence is associated with extratropical cyclones (Villarini, 2016), which combined with the warm humid climate, leads to abundant cool-season precipitation and subsequent flooding (Saharia et al., 2017a; Berghuijs et al., 2016). On a more local scale, flash floods often occur across the southeast US in the winter-spring period due to extreme convective events (Henderson et al., 2020). Over Florida, where six out of ten urban areas most vulnerable to storm surge in the US are located, major flood risk is associated with hurricanes and severe storms, (Cigler, 2017). Furthermore, the southern Appalachian Mountains are considered one of the six hotspots for flash flood formation in the US (Saharia et al., 2017b) due to the combination of abundant moisture and topographic uplift, among other factors. Additionally, the southeast US has and continues to experience substantial anthropogenic changes in landscape structure and characteristics, manifested mainly in increasing urbanization, population growth, and reservoir construction that affects flood risk in different ways (Mogollón et al., 2016).

This article provides an assessment of the spatial and temporal patterns of streamflow peaks identified using an adapted Peak Over Threshold (POT)-based methodology, over the southeast US to quantify occurrences of high-water conditions, which can also be considered a proxy for flood conditions depending on the context of the specific river reach. To provide a wide spatial extent of the analysis and include all important channel routes available within the study area, the

National Water Model (NWM) v.2.1 retrospective data are used. This dataset comprises simulated streamflow information for the period 1979–2020, and while the data are only verified at select river locations (Hodson et al., 2022), the consistent temporal resolution and high density of data points allows the data to be used to define general spatial and temporal hydrologic characteristics across the Southeast US study area. As research has shown that variations in extreme streamflow are related to environmental characteristics along with atmospheric factors, such as geology, land use, urbanization, or snow conditions (e.g. Apollonio et al., 2016; Carlier et al., 2018; Kazakis et al., 2015; Oudin et al., 2018; Zope et al., 2016), due to spatially different forcing conditions implemented in the NWM model (fig. 1), the primary objective of this study is to define the ability of the NWM to identify spatial and temporal patterns of streamflow peaks reflected in local environmental characteristics (fig. 1). Building on these findings, the secondary objective of the work is to quantify changes in peak streamflow parameters (e.g., values and volumes) over the NWM period of record. The results of these objectives will provide important information on the patterns and trends of peak streamflow across the Southeastern US, and will highlight the viability of the NWM distributed hydrologic model as a tool to provide a spatially and temporally continuous dataset for assessing long-term streamflow patterns.

2. Material and Methods

2.1. Study Area

The study area for this project is the southeastern US, defined by the US Geological Survey (USGS) Region 3 boundaries that describe the South Atlantic-Gulf (SAG) hydrologic unit. The SAG region includes all rivers between the Lower Mississippi River in Mississippi and the James River catchment in Virginia that flow into the Gulf of Mexico and Atlantic Ocean (fig. 1). The total area of the region is around 724,000 km^2 and consists of a diverse natural landscape, elevation varying between -25–1589 m a.s.l., multiple land use and vegetation types, and a broad range of geological, hydrological, and meteorological conditions. Cretaceous and Quaternary aquifers have a daily discharge of around 0.3 km^3 and move generally toward the Gulf of Mexico and Atlantic Ocean, which is reflected in the layout of river networks (Cederstrom et al., 1979). The climate is primarily subtropical with mild and wet winters and hot and dry summers, except along the Gulf Coast and into Florida where the climate shows a more tropical pattern. Annual precipitation ranges between 1000–2000 mm and mean annual temperature varies between 14°C–25°C (Joshi

et al., 2020; Sagarika et al., 2015). Streamflow discharge and water resources are affected by precipitation and evaporation, with general circulation patterns controlled mainly by the El Niño-Southern Oscillation (ENSO) (Abtew & Trimble, 2010; Adusumilli et al., 2019; Clark et al., 2014; Mourtzinis et al., 2016; Sagarika et al., 2015). Despite the abundant precipitation, water resources are limited by increasing industrial and residential water demands as well as agricultural irrigation (Cook et al., 2020; Keellings & Engström, 2019; Marx et al., 2018).

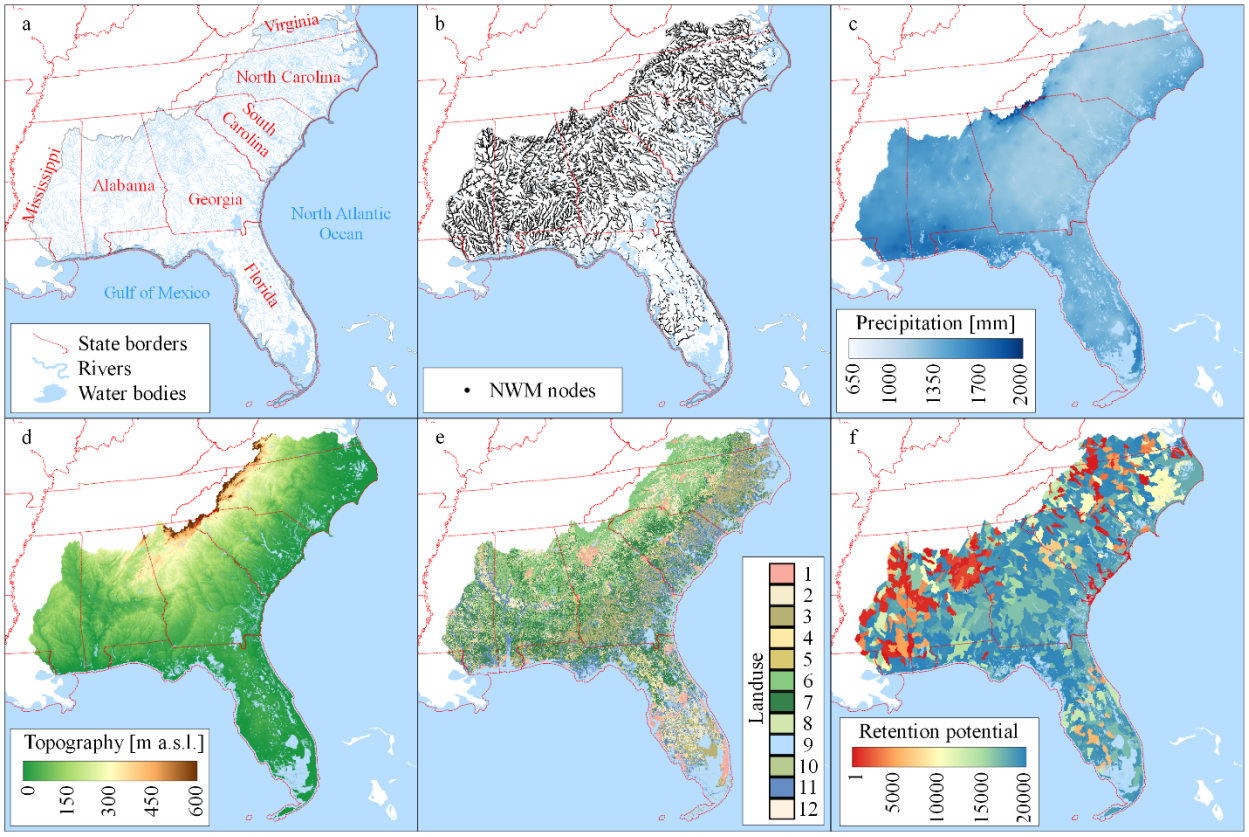

Fig. 1. Study area overview (a) and NWM stream segments (nodes) location (b) used for analysis, as well as main environmental characteristics: mean annual precipitation (c), topography (d), land use (e) based on the classification used for NWM setup (1 - Urban and Built-up Pasture, 2 - Dryland Cropland and Pasture, 3 - Irrigated Cropland and Pasture, 4 - Grassland, 5 - Shrubland, 6 - Deciduous Broadleaf Forest, 7 - Evergreen Needleleaf, 8 - Mixed Forest, 9 - Water Bodies, 10 - Herbaceous Wetland, 11 - Wooded Wetland, 12 - Barren or Sparsely Vegetated), and retention potential index (f) used in NWM setup (a higher value means more water will stay on the surface before being routed through overland flow processes); please refer to Supplementary Materials for a high resolution digital version of this figure

2.2. Datasets

The National Water Model (NWM) was developed and released in 2016 by the National Oceanic and Atmospheric Administration (NOAA) for the purpose of improved modelling and forecasting of floods. The NWM products come with operational and retrospective configurations, with the former including current forecasts of streamflow in various temporal configurations (e.g., short and medium range timeframes), and the latter providing historical flow reconstruction. The NWM is based on the Weather Research and Forecasting – Hydrological Modeling System (WRF-Hydro), and contains 2.7 million river reaches over the CONUS, with a 1-km land surface grid for land surface modeling and 250-m grid for surface and subsurface runoff routing. Version 2.1 of the model, which is used in this study, incorporates forcing data from the Office of Water Prediction Analysis of Record for Calibration (AORC) dataset (Cosgrove et al., 2019). Within the NWM, the SAG region contains over 338,000 individual stream segments (hereafter referred to as nodes) where simulated discharge is provided.

The NWM retrospective dataset (v.2.1) was used in this study for the entire historical timeframe available (Feb. 1979-Dec. 2020). Model calibration/validation was performed before product release by NOAA (independent to this study), and was based on around 1400 calibration basins against hourly streamflow observations (Blodgett, 2022; Gochis et al., 2018). This includes 715 USGS gauges within the southeast US, which were used as streamflow benchmark locations for the NWM model (Foks et al., 2022; Hodson et al., 2022). Validation studies indicate a good performance of the model within higher flow ranges, with some evidence of lower performance for low flows (Garousi-Nejad & Tarboton, 2022; L. E. Johnson & Kim, 2019; Rahman et al., 2022; Towler et al., 2022; Wan et al., 2022). For additional verification of the data specifically used in this study, the daily, monthly, and annually aggregated data series available in NWM nodes were compared to USGS observation data over the same aggregated time periods. The USGS observed dataset consisted of of 520 gauges located across the southeastern United States for which daily flows were available between Jan 1995 and Dec 2018, which is the longest time series available before the number of viable stations decreased substantially. The gauge data were compared with the closest NWM node in terms of spatial distance, and the series means were extracted pairwise such that gauges with an overall flow ratio between 0.5 and 2 were used for correlation analysis (to exclude pairs of points on unrelated segments, in total 439 pairs). The

comparison between the NWM simulated and USGS observed data pairs showed correlations $r \in$ <0.7; 0.9> for daily flows, $r > 0.75$ for monthly series and $r \in$ <0.7; 1.0> for annual data. The associated Kling-Gupta efficiency that provides a goodness-of-fit measure were above the threshold value, with means close to 0.5 (fig. 2). When only the upper range of the flow duration curve (FDC) was considered (highest flows, constituting 35% of the data), the relations remain similar.

To maximize the temporal continuity of the NWM data, nodes were analyzed for percentage of missing data. More than 80% of nodes of Strahler order one or two contained long series of missing or 0 values, and therefore were excluded from the study. After further evaluation of data homogeneity, which included a Grubbs test for outliers (Komsta, 2006), data independency series test (Wald & Wolfowitz, 1942) and stationarity assessment (Yue et al., 2002), a decision was made to include in the analysis only nodes of Strahler order three and higher, with additional criteria of at least 95% of the data series at any node being non-zero. This approach resulted in 61,948 nodes retained for this analysis (fig. 1), for which daily mean flow (00z-00z) was calculated based on the hourly values provided in the retrospective dataset. The final dataset consisted of daily average flows for a period from 1-Feb 1979 to 31-Dec 2020 (2,601,816 stream years).

Average monthly and annual precipitation data used in this study were obtained from the U.S. Federal Government Climate Resilience Toolkit (U.S. Federal Government, 2014).

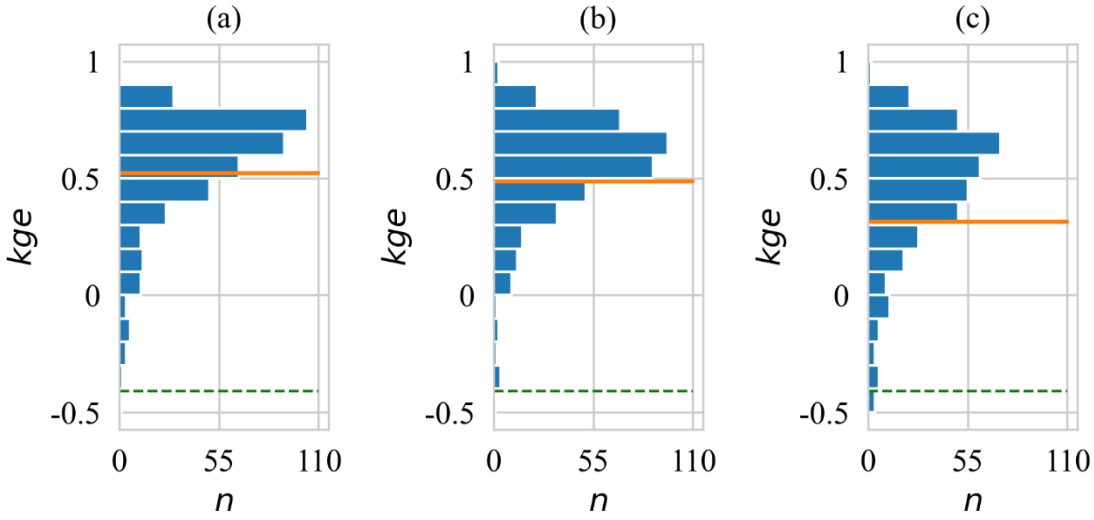

Fig. 2. Distribution of Kling-Gupta Efficiency (*kge*) between USGS observations and associated NWM nodes, visualized as number of pairs *n* with measure at specified level for daily (a),

monthly (b) and annual (c) data series; mean value marked with orange line and measure threshold value marked with green dashed line

2.3. Streamflow peaks identification

The term *flood* is defined in various ways, depending on the context and study objectives. In anthropogenic terms, it refers to the excess of water that poses a risk to human life and property, while in natural conditions, it refers to high water levels in a river channel that can result in inundation of adjacent areas if the bank level is exceeded. In general, though, different definitions and criteria are used to define floods, tailored to the specific needs of the study or impact criteria, although the occurrence, intensity, and direction of flood development are closely associated with increased, high, or maximal streamflow. Therefore, analyzing these characteristics is essential to understanding the nature of floods. One method applied in flood frequency analysis to identify potential flood-generating streamflow conditions is the Peak Over Threshold (POT) method. In this approach, peak flows exceeding a defined threshold value are considered flood peaks (f.e. Önöz and Bayazit, 2001; Eastoe and Tawn, 2010; Pan and Rahman, 2022). In this research, a POT-based approach was applied to the NWM retrospective streamflow data to identify periods of increased river discharge. Following this method, a threshold level is predefined, and all flows higher than this threshold are considered streamflow peaks (hereafter referred to as SFP), which depending on the level of streamflow and other hydrologic conditions as well as societal impacts, can be referred to as flood events (f.e. Burn et. al., 2016). Due to the character of this study, however, the naming from this point on is limited to streamflow peaks, which describe the series of flows above the adopted threshold, representing the increased water availability in a river channel (as presented in fig. 3) with no consideration of the associated societal or environmental risk of the increased flows.

Various thresholds have been applied in previous studies, usually constituting a high criteria percentile derived from a flow duration curve (FDC) such as the 90^{th}, 95^{th}, or 99^{th} percentile (f.e. Casse et al., 2015; Paltan et al., 2017; Tramblay et al., 2019); however, applying a single, unified value as a threshold level is not representative for higher flow conditions across a region, and often results in variations of calculated flood hazard (Prime et al., 2016). Additionally, the percentile approach does not provide event-based information, which might be considered in different methods, but is usually not transferable across different locations (Stein et al., 2020).

From a numerical perspective, percentiles calculated based on a FDC derived from model data (like the NWM) might be affected by data discretization errors such that extreme flow values may not vary continuously. Unlike in the case of observational datasets, the modelled data are limited by the parametrization of the model based on estimated environmental conditions. Although this issue is observed more often in low flow values (Raczyński and Dyer 2022), it might occur within higher flow ranges if unfavorable modeling conditions occur. To avoid such scenarios and exclude uncertainty associated with subjective researcher decision on threshold percentile level (Pan and Rahman, 2022), a breakpoint approach was used to generate thresholds for each streamflow node separately. In this approach the unique shape of a node's FDC is considered when determining peak threshold, which allows for the inclusion of environmental factors in the decision-making process. Like low flow conditions, significant changes in FDC shape indicates a potential change in local conditions that corresponds to changes in flow distribution in the river channel. In the case of low flows, such a change in the lower range of the FDC indicates a moment of change from precipitation-based supplementation to groundwater-based supplementation of runoff, indicating the onset of hydrologic drought (Raczyński and Dyer 2022). In the upper range of the FDC this level might indicate bank-level flows or extreme precipitation conditions, relating to increased runoff due to complete saturation of the soil or reaching the limit of catchment retention abilities.

To objectively determine the threshold (Q_{obj}) at each node, the Fisher-Jenks natural breakpoint algorithm is used over the upper range (35%) of the FDC (Raczyński and Dyer 2022). The flow at a specific node is considered a SFP when its value exceeds the value of Q_{obj} defined for that specific node.

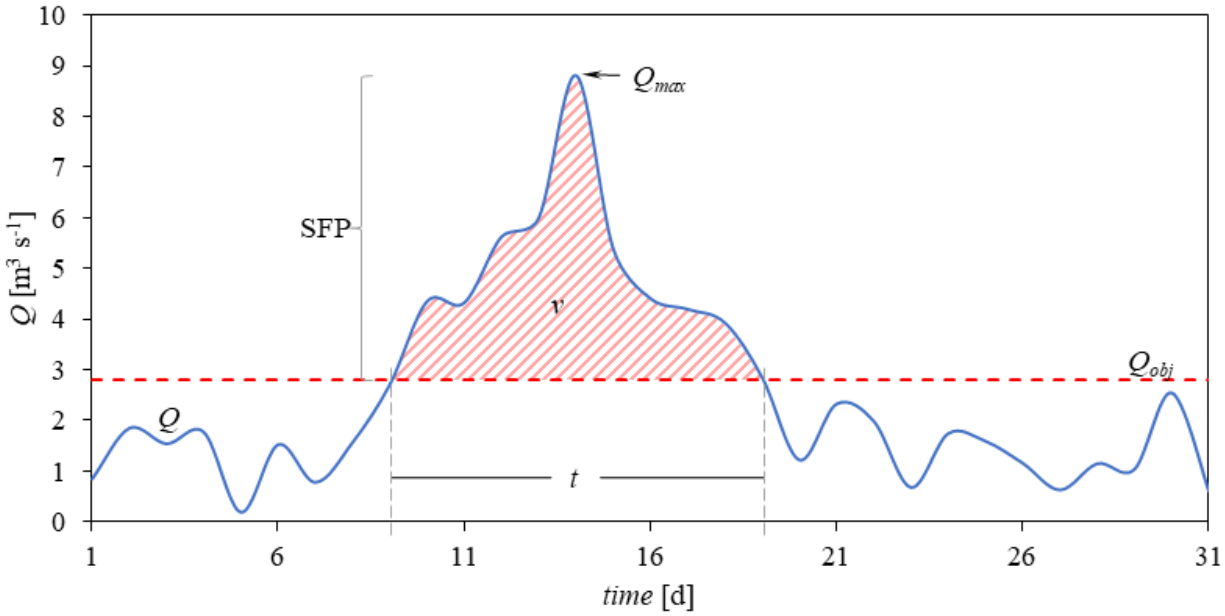

Fig. 3. Streamflow peak (SFP) is identified when flow values exceed a predefined threshold (Q_{obj}). Main parameters of SFP are Q_{max} – maximum flow/peak value [m^3 s^{-1}], v – volume [m^3] and t – duration [d]

In the majority of cases the value of Q_{obj} falls between the 97.5th and 99th percentile (fig. 4), indicating that most of the significant FDC breakpoints appear in the highest range of flows, with thresholds close to the 50- or 100- year return interval. This indicates that peaks identified in this study correspond to severe flooding conditions, which are generally represented by the values of the FDC above the 95th percentile (Tramblay et al., 2019). In this study only 74 nodes (0.119%) were characterized with a breakpoint level lower than the 90th percentile, including eight cases being lower than the 85th percentile.

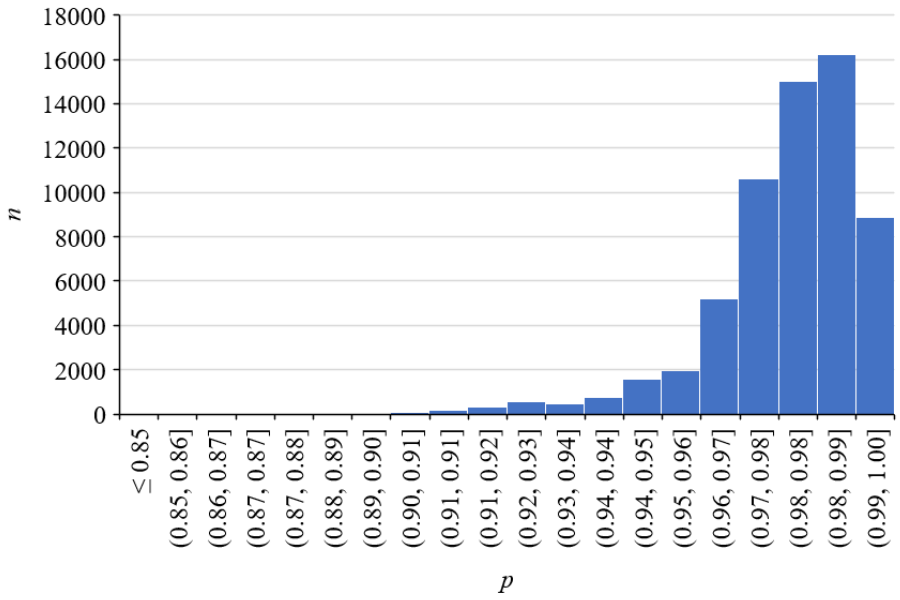

Fig. 4. Number of nodes n with Q_{obj} thresholds identified by an objective approach, with the threshold value presented as a probability value equivalent across all NWM study nodes

Identified peaks were parametrized to include their duration times (t, fig. 3) and volumes (v, fig. 3). SFP characteristics were aggregated in monthly, annual, and total (entire study period) intervals.

The flood event duration (t) is the difference (in days) between the day when Q_{obj} was reached for the first time in the sequence (beginning of flood episode) and the subsequent day when flow falls below Q_{obj} (flood episode end) (fig. 3).

The SFP volume (v) is calculated as the difference between the hydrograph and the threshold:

$$v = \int_{t_b}^{t_e} (Q - Q_{obj}) dt \quad (1)$$

where: Q – flow [$m^3\ s^{-1}$]; Q_{obj} – objective threshold [$m^3\ s^{-1}$]; t_b – day of the beginning of the flood; t_e – day of the end of the flood.

While the durations can be directly compared between all nodes, due to the same unit and event scale, the volumes relate to the total river outflow (and therefore partially refer to stream order) and cannot be directly compared between all study nodes. To address this issue, the ratio of volume to total river outflow (Q_f/Q_t) for each node was calculated, as:

$$Q_f/Q_t = \frac{v}{\sum_{i=1}^{n} Q_i \cdot 86400} \cdot 100 \quad (2)$$

where: Q_f/Q_t – share of SFP volume in total outflow [%]; v – SFP volume [m^3]; n – number of days in series representing the SFP; Q_i – flow in day i [$m^3\ s^{-1}$].

In addition to SFP characteristics, a maximal flows (Q_{max}) analysis was performed. These values were aggregated in annual and monthly intervals to avoid the problem of multiple peaks occurring in the same aggregation step.

2.4. Statistical Analysis

The trends in the individual data series at each node were determined using the nonparametric Mann-Kendall (MK) test with Hamed and Rao modification for seasonality applied for series representing monthly data (Hussain & Mahmud, 2019). The test null hypothesis states that there is no monotonic trend in the data. If statistically significant trends are present in the series, Sen's slope was used to determine trend direction and magnitude, with positive (negative) values indicating increasing (decreasing) trends. Sen's slope represents the median of slopes for lines through pairs of points, and its value provides an estimate of value change (increase or decrease) over the predictor unit step. For example, for annual data with a significant trend, a Sen's slope of $S = 0.2$ means that there is a statistically significant increase of 0.2 units (by median) per year in that parameter. Sen's slope usually does not represent the exact value of change, as it is not constant in time, but provides an accurate estimation of its general value over the entire series. As trends are highly dependent on the data resolution, a two-directional trend volatility analysis was performed with a fixed starting date and flexible ending date (and vice versa). This was done under the assumption that the shortest tested data series will not be shorter than ten values as the power of the MK test is an increasing function of the series length (Wang et al., 2020).

To determine spatial relationships between nodes with similar characteristics, a *K*-means clustering was applied. The algorithm is used to group similar data into clusters by minimizing the objective function *J(z,A)* with updated cluster centers (Sinaga & Yang, 2020):

$$J(z, A) = \sum_{i=1}^{n} \sum_{k=1}^{c} z_{ik} \|x_i - a_k\|^2 \quad (3)$$

where k is cluster number, c is number of clusters, x_i is the data point, a_k is center of cluster k, and z_{ik} is a binary variable that indicates if the data point is considered within the cluster k. The optimal number of clusters is determined based on the "elbow" method, in which the model is fitted to a range of c, and the point of curve inflection (so called "elbow") indicates the optimal c.

In this study, all relations between variables were assessed using the Spearman rank correlation coefficient *r*. Spearman rank correlation is a non-parametric statistical test that measures the strength and direction of monotonic association between two variables, making it useful when the variables being analyzed are not normally distributed or when outliers may be present. All computed statistics were performed assuming a two-tailed distribution with $\alpha = 0.05$.

3. Results

3.1. Characteristics of streamflow peaks

The number of SFPs defined over the 42-year study period among the streamflow nodes retained for analysis ranges from a median of roughly 100 episodes to a maximum of over 350 episodes (fig. 5). This translates to an average of 2.4 SFPs per year over all the stream nodes. Most frequent occurrence is in headwater streams, especially in the Appalachian Mountains and piedmont river sections, while the lowest number of SFPs occur near major river outlets along the Atlantic and Gulf Coasts (fig. 6).

The distribution of total durations was highly skewed, with a median of 285 days and an interquartile range (IQR) of around 200–450 days (fig. 5). The highest number of days with SFPs occurred in the central part of the study area, from southwestern parts of South Carolina through Georgia to central Florida, while the lowest number occurred in the coastal region of North Carolina (fig. 6).

The majority of total volumes are within 10^8–10^9 m^3, with a median around 1.64^8 m^3 (fig. 5), with the highest values (exceeding 10^9 m^3) related to peaks within the region's largest river systems.

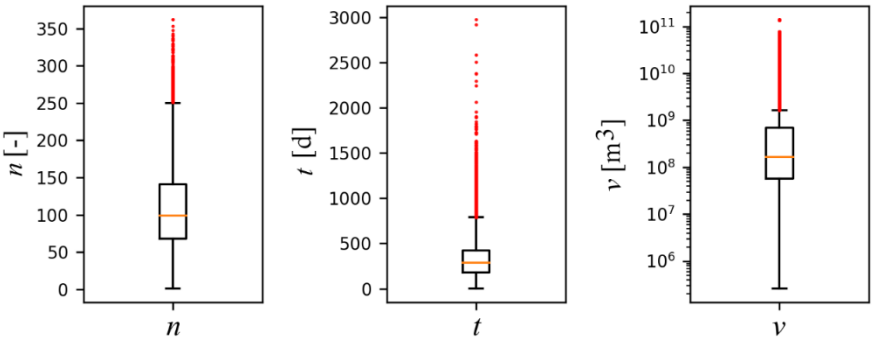

Fig. 5. Number of SFPs *n* during the study period, total duration *t*, and total volumes *v* in all studied nodes. Orange lines indicate median, and red points are outliers (+/- 1.5 IQR)

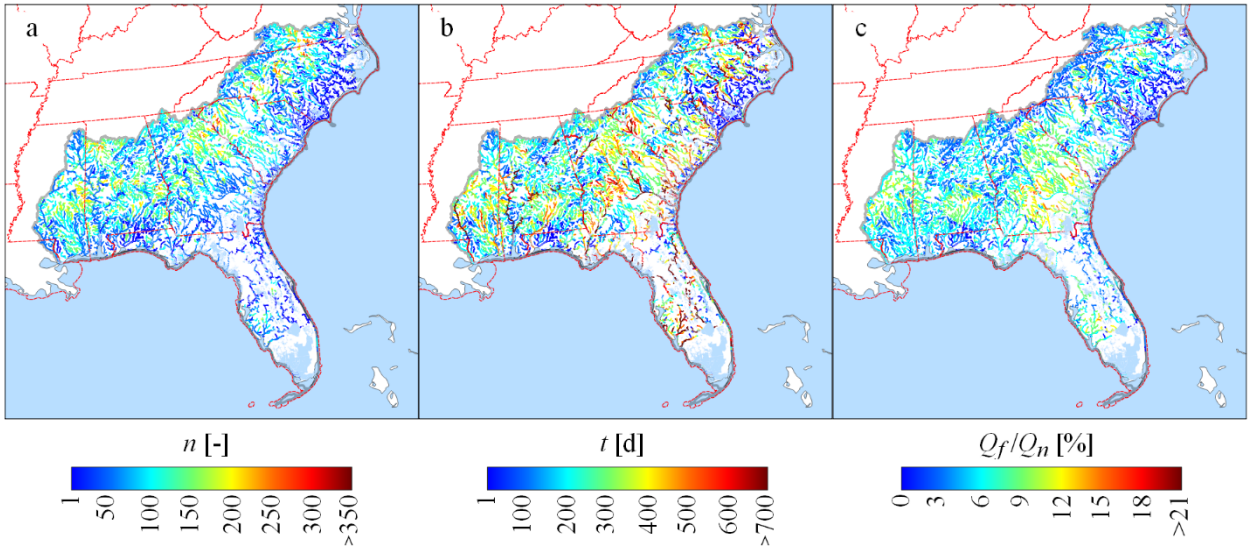

Fig. 6. Spatial distribution of SFP parameters in studied nodes accumulated as totals over the study period: number of SFPs n, duration t, and volume share in total runoff Q_f/Q_t

The relation between SFP duration and volume is statistically significant; however, the relationship is weak ($r = 0.46$) due to the high variability of volumes in smaller rivers. This results in high spread in the lower part of the distribution (low SFP volumes) and a corresponding narrowing of volume distribution in the upper part due to the lower number of higher order rivers (fig. 7). For higher volumes this relation is stronger (fig. 7), which reflects the geometric decrease in the number of nodes with increasing stream order. Volumes (v) correlate with total runoff (Q_t) at $r \approx 0.99$.

Spatially, the contribution of SFP volume to total discharge is highest in the central part of the study area, where in southeastern Georgia the ratio of Q_f/Q_t exceeds 15% and for south Alabama and central Mississippi the value ranges between 9–15%. The lowest share of SFP volume in total discharge is observed through coastal North Carolina and the western Florida Panhandle (fig. 6). North Carolina can be considered an area with the lowest share of SFP volume in total discharge (less than 3%), with only two river systems – the Tar River and Cape Fear River – exceeding 6%. Most of the biggest rivers in the study area have higher Q_f/Q_t ratios in the upper parts of their respective catchments (corresponding with lower Strahler stream order), which then decreases downstream as basin area increases.

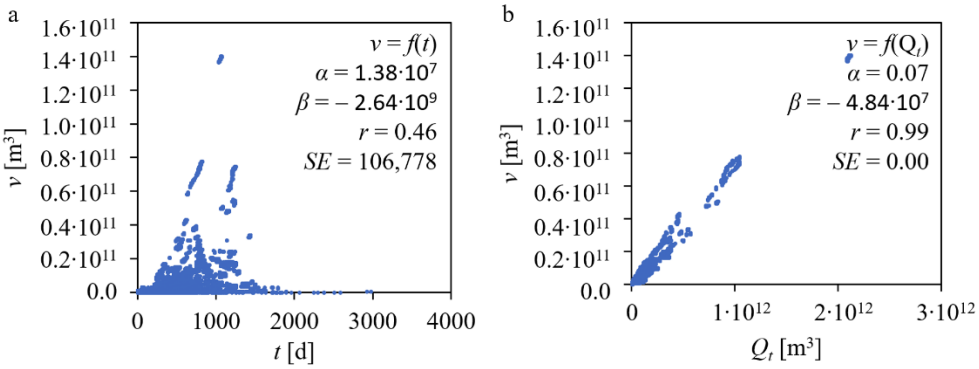

Fig. 7. Relation between SFP durations t and volumes v (a) and volumes and total discharge Q_t (b) with parameters of linear regressions; α – slope, β – intercept, SE – standard error.

3.2. Annual and Monthly Variability

The highest frequency of SFPs over the southeast US occurred between 1989-1998 and 2013-2020, with between four and six episodes on average over all stream nodes (fig. 8). The statistical distribution of SFP durations roughly follows the distribution of frequency; however, there are some nodes for which increased SFP duration (t) reaches over 300 days in years 2003-2005 and 2018-2020. Although an almost annual occurrence of SFP is apparent based on frequency and duration, the distribution of SFP volumes reveals when significant peaks occurred, namely in 1980, 1983, 1990, and 2020 (fig. 8). The SFP volumes follow the annual distribution of outflow, with the correlation coefficients between the two series varying from r=0.96 for 2020 to r=0.04 for 1981, with all correlations being statistically significant (with nine values of r<0.4 and 15 values of r>0.8).

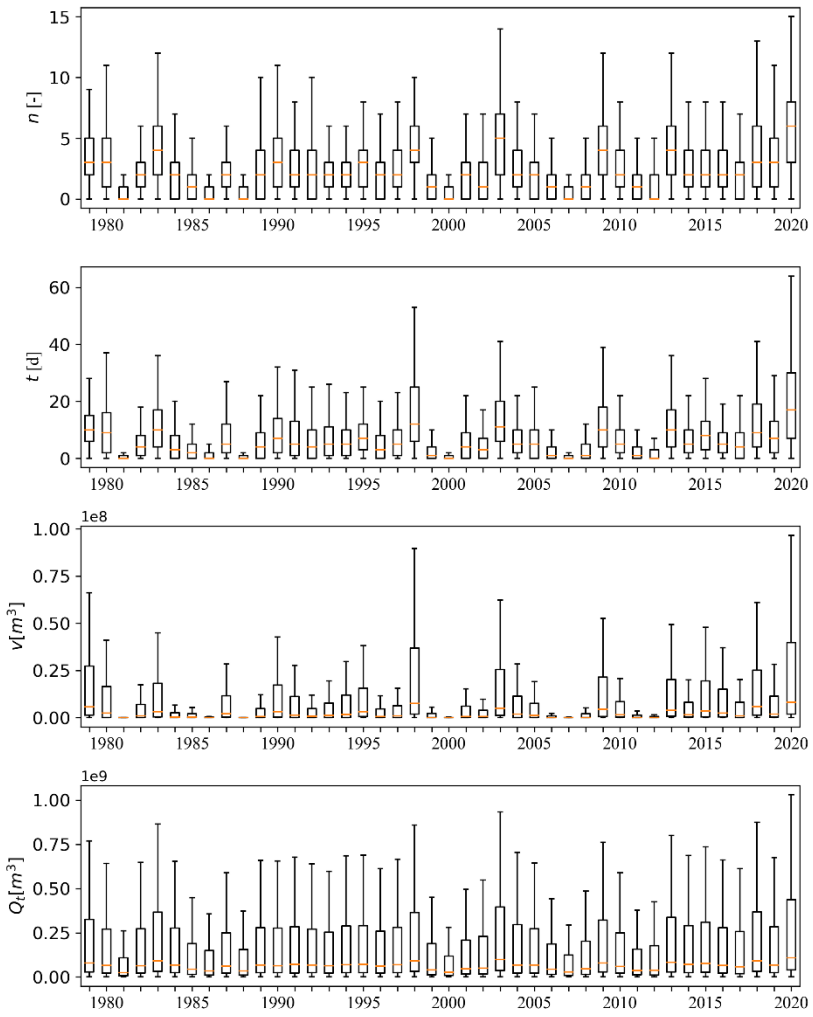

Fig. 8. The annual distribution of SFP parameters over the study period: frequency *n*, duration *t*, volume *v*, and total runoff Q_t; outliers (+/- 1.5 IQR) are excluded

The spatial distribution of annual SFP occurrence reveals three general clusters based on the results of the K-means clustering approach. SFPs in Mississippi through northeastern Alabama, defined as the first cluster, occurred mainly during three periods (1979-1983, 1990-1991, and 2019-2020). The second cluster, over southeastern Alabama, Georgia, and southwestern South Carolina showed a higher persistence, with comparable year-to-year occurrence of peaks and two low-frequency periods between 1981-1985 and 2004-2008. The third cluster, covering Virginia, North Carolina, northeastern South Carolina, and Florida, indicate SFPs occurred with a roughly 10-year cycle and low intra-annual persistence as well as an increase in occurrence in recent years (fig. 9).

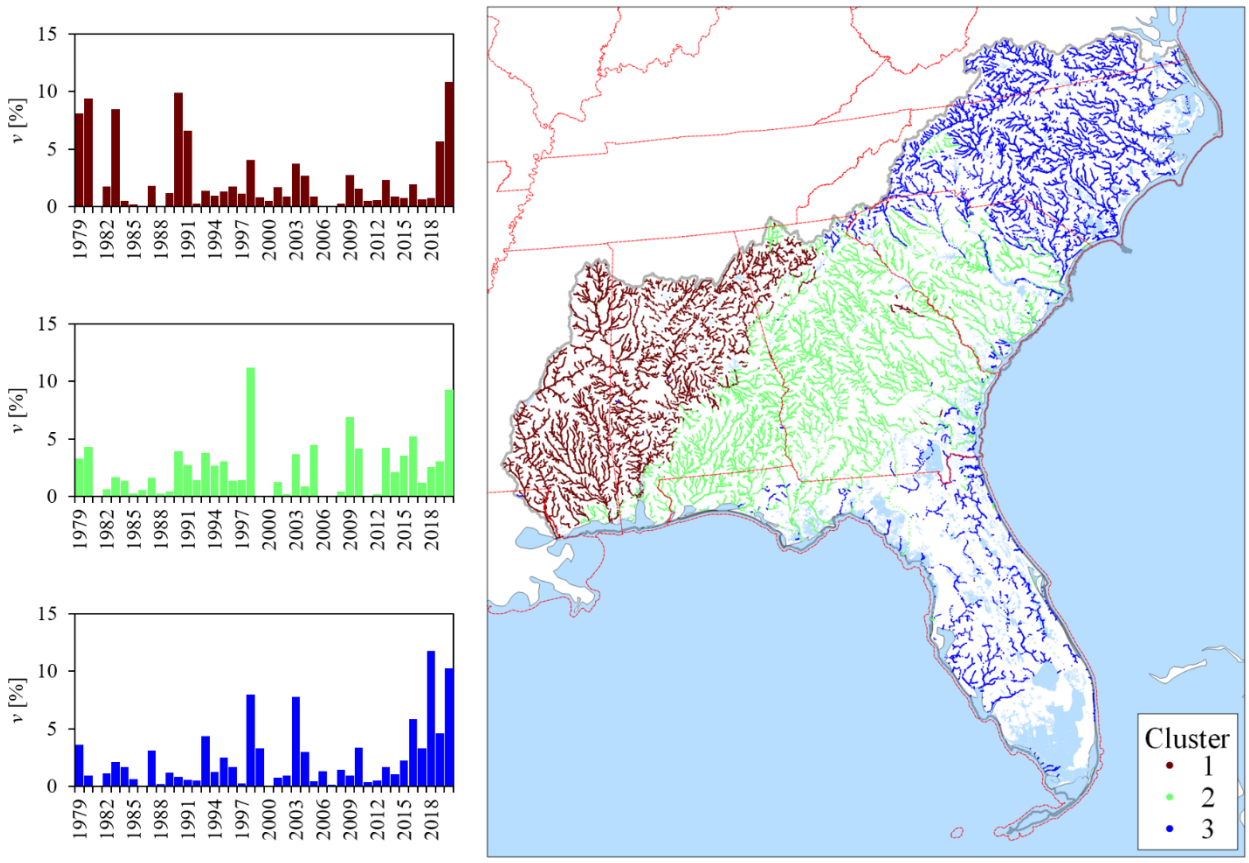

Fig. 9. Spatial clustering of nodes with similar patterns in annual occurrence of SFP, represented by normalized node volumes aggregated in annual intervals (a) with annual sums of these volumes in each identified cluster: cluster 1 (b): east Mississippi and northwest Alabama; cluster 2 (c): southeast Alabama, Georgia, and South Carolina; cluster 3 (d): Florida, North Carolina and south Virginia

The spatial patterns of annual SFP distribution are further reflected at the monthly scale. For most nodes, from Mississippi to South Carolina, peaks occur most frequently during the late winter/early spring months (January-April) (fig. 10), which follows the pattern of monthly total discharge based on the regional subtropical climatological conditions (wet winters and dry summers). The correlation between v and Q_t is statistically significant and reaches the highest scores in January-March (r>0.7) and lowest in August (r=0.21), with correlation coefficients in the warm months (June-October) of $r \leq 0.5$. This relates to the seasonal distribution of precipitation for the majority of nodes, such that nodes located along the Gulf Coast or in Florida receive the

most precipitation in the warm season, while peaks at nodes further inland occur during the cool season when precipitation is highest in the respective areas.

Spatial clustering for the monthly distribution of SFP volumes is ambiguous with two breakpoints of the curve indicating division into two and/or four clusters. The first cluster constitutes nodes over the central region, from Mississippi to South Carolina (fig. 10), where peaks occur from December to April with highest frequencies in March. In this group, peaks during the warm season are rare. The second cluster consists of nodes along the Gulf Cost, Atlantic Coast, Florida, and parts of the eastern study area (fig. 10), where maximal occurrence is shifted to September and October with a smaller secondary peak in February-March for southern nodes. This generally corresponds to the tropical climate zone within the southern edge of the study area. In the Florida and Gulf coast regions a higher frequency of SFPs occur during the warm period, which corresponds to the wet season. In case of further clustering into four groups, the third and fourth clusters are extracted as subclusters of the second, and constitute nodes located in coastal areas of the Carolinas and Georgia. In these clusters, SFPs occur only during the September-October time frame. In the third cluster, consisting of nodes through the coastal region of North Carolina, SFPs occur mainly in September (~80%). In the fourth cluster, consisting of nodes along the Atlantic Coast in South Carolina, Virginia and partially Georgia, the occurrence is shifted to late September and October (fig. 10).

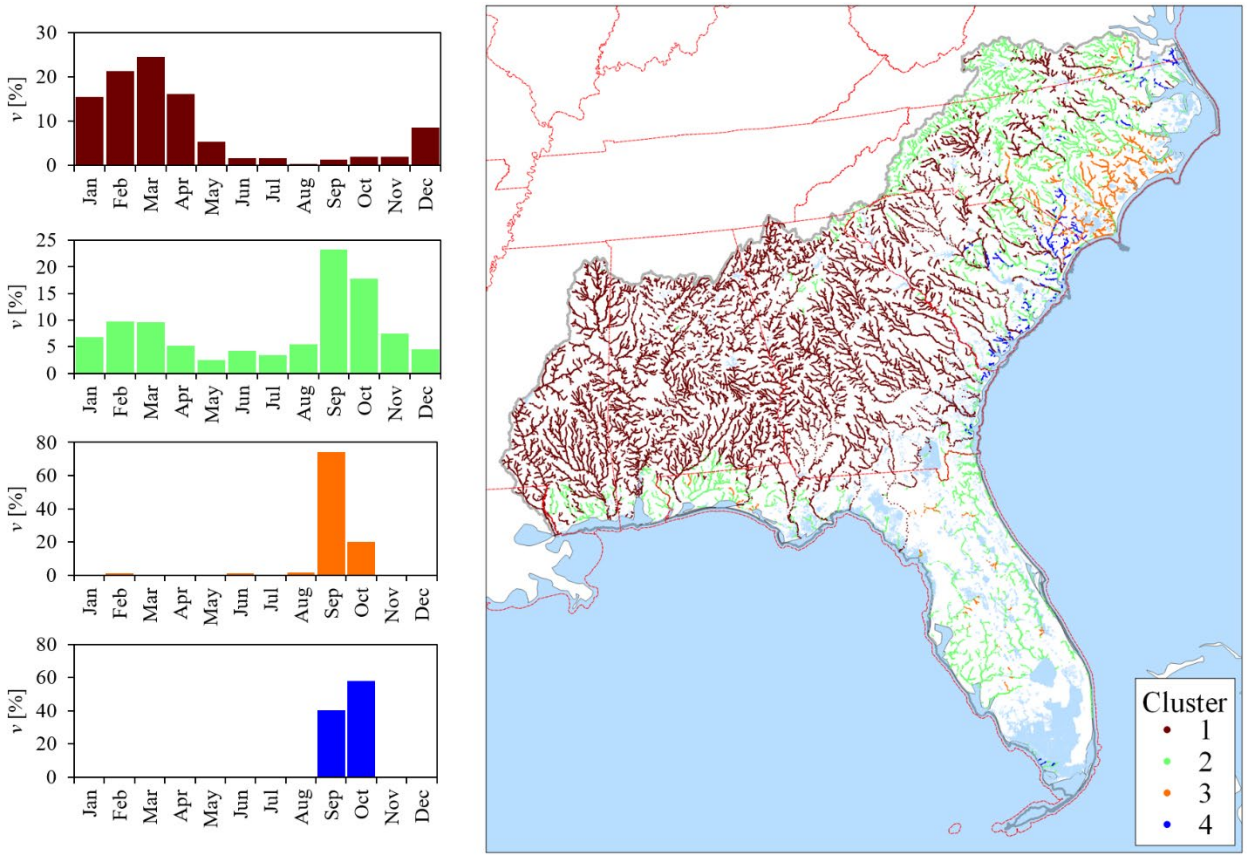

Fig. 10. Spatial clustering of nodes with similar patterns in monthly distribution of SFPs, represented by normalized node volumes (a) with monthly share of these volumes in total annual volume for each cluster: cluster 1 (b): east Mississippi, Alabama, Georgia, and southwest South Carolina; cluster 2 (c): Florida, Gulf coast, North Carolina, and Virginia; cluster 3 (d): Atlantic coast in Carolinas; cluster 4 (e): Atlantic coast in Georgia, Carolinas and Virginia

SFP distribution generally follows the 100 mm isohyet in the cold season and 150 mm isohyet in the warm season (fig. 11). From January through April the highest precipitation occurs between Mississippi and Georgia, with monthly averages exceeding 125-150 mm. This area corresponds to the spatial cluster with the highest SFP occurrence, with mean volumes over the study period exceeding 3.5 billion m^3 per node (compared to mean volume of 107 million m^3 per node for the cluster with the lowest frequency over the same period). During April and May, the area of highest precipitation moves north-west and SFPs in the region begin to decrease, while between June and September they occur mainly over Florida where the highest precipitation occurs in the warmer months due to the tropical climate. Starting in October, precipitation starts to

increase over inland areas and decreases over Florida and the Gulf Coast, and the SFP occurrence patterns begin to change again in an east-to-west direction (fig. 11). For the northeastern part of the study area, including stream nodes in Virginia and the Carolinas, two periods of increased SFP frequency are present during February-April and September-November.

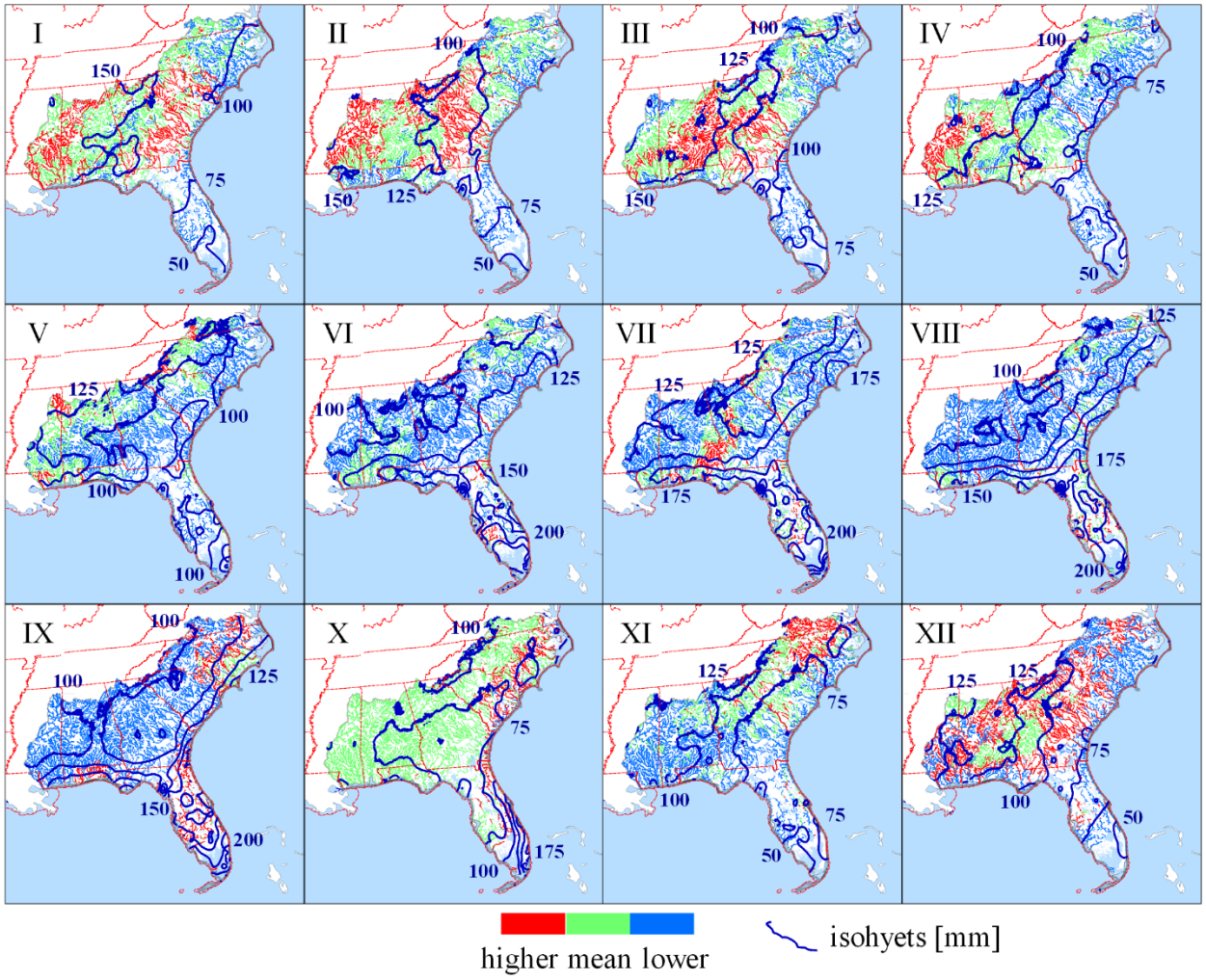

Fig. 11. Spatial clusters of nodes based on monthly SFP occurrence and isohyets of mean monthly precipitation over the study area. Cluster description (higher, mean, lower) indicates relation to SFP occurrence for the respective month in other clusters.

3.3. Trends

Trend analysis indicates that there are three main regions where statistically significant changes in SFP magnitude occur over the 1979-2020 study period. All three regions in central

Florida, southwestern Georgia through southeastern Alabama, and North Carolina show statistically significant increases in SFP volumes (fig. 12). Increases in most nodes are around 100,000 m^3 y^{-1} for Georgia-Alabama and North Carolina nodes, and 100,000-600,000 m^3 y^{-1} for nodes in central Florida (fig. 12). For the three abovementioned regions, a statistically significant increasing trend of maximal annual flows was also found (fig. 12), with most nodes indicating an increase at or below 1.5 m^3 s^{-1} y^{-1}.

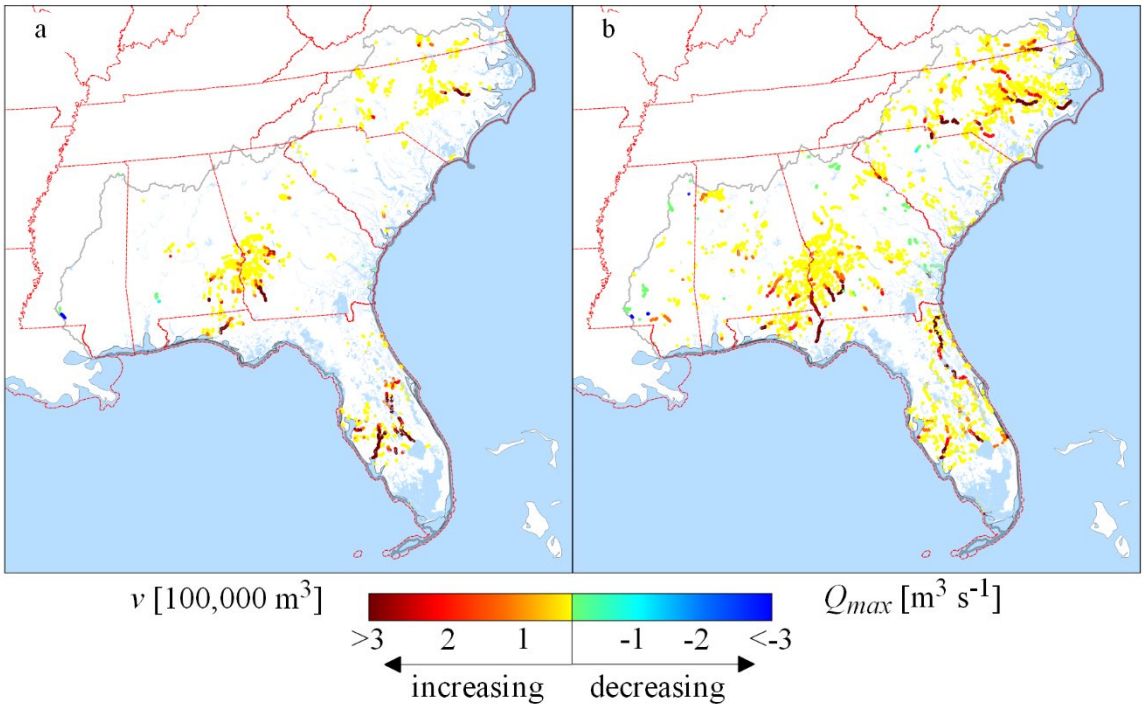

Fig. 12. Statistically significant trends over the 1979-2020 study period for annual SFP volumes v (a) and maximal flows Q_{max} (b) represented by Sen's slope value

Trends are often dependent on the timeframe of the studied series; therefore, to verify observed relations, a trend volatility analysis was performed. Areas of Georgia, Alabama, and Florida maintain increasing tendencies in over 150 combinations of time scales (about 24% of the total possible combinations; fig. 13). Strong increasing trends of SFP magnitude are present in these regions between 1980-2000, and any time series combination ending in recent years (fig. 13). This indicates that SFP magnitudes are increasing in recent years. The decreasing trends occur mainly in the coastal areas of the Carolinas, and occur in 50-100 timeseries combinations (8-16% of the total), especially in the early 1980's. The Appalachian Mountains region indicates some

significant decreasing changes over the 1989-2010 period, which could be partly due to an increased number of reservoirs along with other changes to meteorological and surface conditions (e.g. Mogollón et al., 2016) (fig. 13).

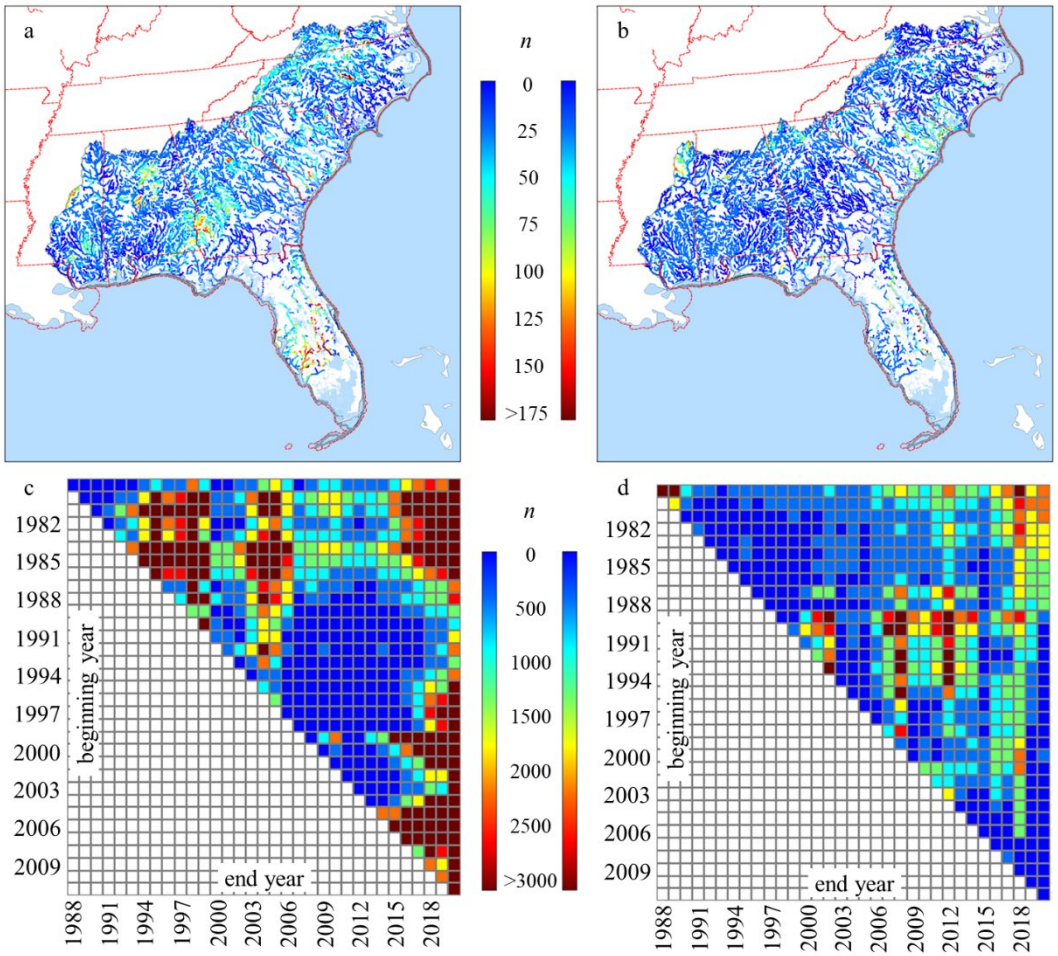

Fig. 13. Number *n* of statistically significant increasing (a) and decreasing (b) trends in studied nodes and trend volatility analysis for statistically significant trends depending on the data resolution presented as number of nodes *n* with statistically significant increasing (c) and decreasing (d) changes

Despite the low number of statistically significant trends in monthly SFP volumes over the three regions discussed above, the monthly series of maximal flows indicates changes over the entire study area (fig. 14). From this, three main spatial areas can be distinguished based on trend directions. The first is a latitudinal belt stretching from the Gulf Coast in Alabama through northern

Florida to the Atlantic coast of North Carolina, where statistically significant decreasing trends are present in every month (fig. 14). The second area is located north of this belt, where increasing trends are present mainly in the May-January period. The third group constitutes nodes located in Florida, where the trend direction depends on the month, with decreases present in the western part of the area from March to September and increases present in the east from June to January (fig. 14). The highest increases in maximal flows over the study area are present between August and October.

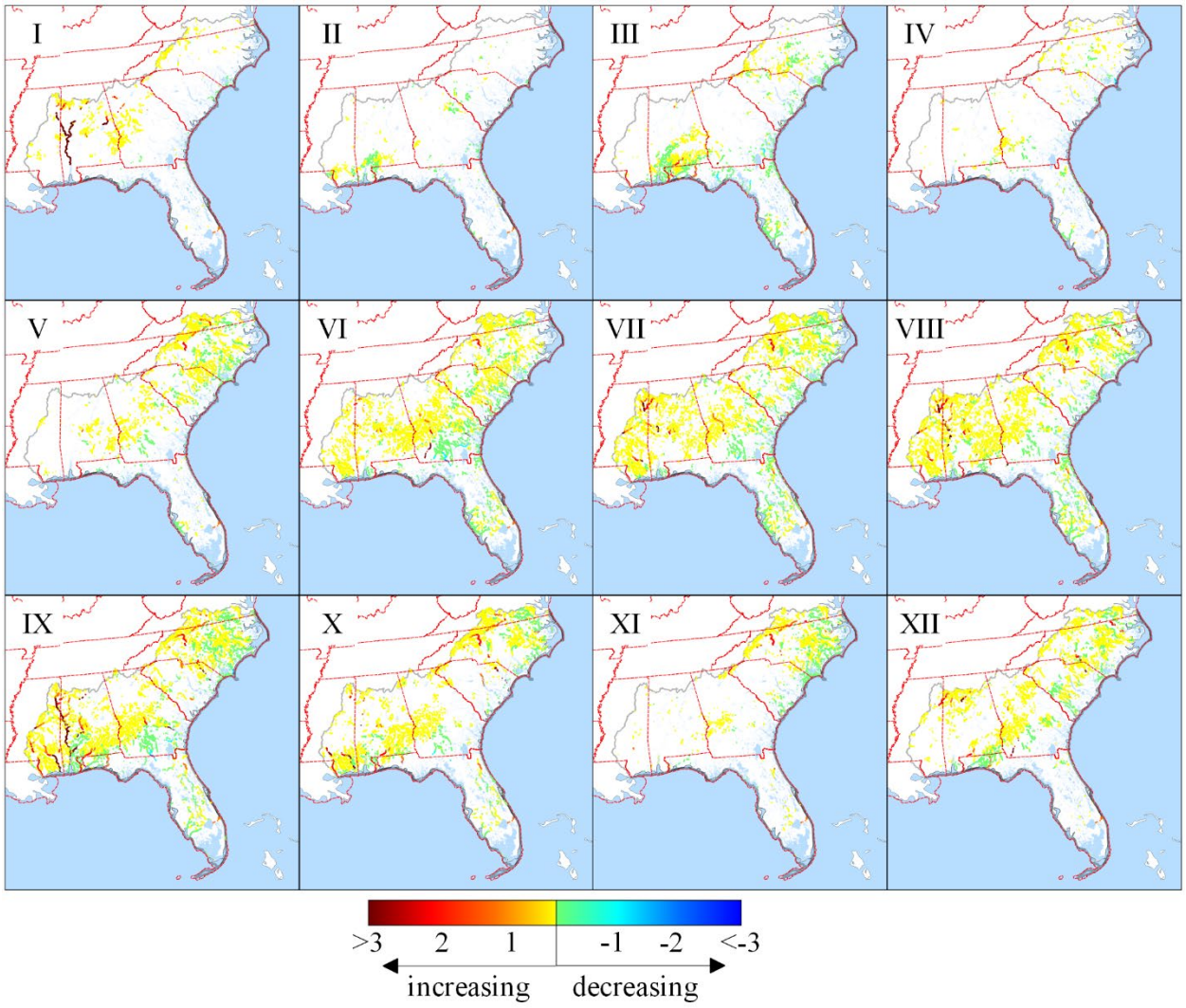

Fig. 14. Statistically significant trends in monthly maximal flows [m^3 s^{-1}] over the 1979-2020 study period represented by Sen's slope value

4. Summary and Discussion

High streamflows in the southeastern United States are driven primarily by excessive rainfall (Berghuijs et al., 2016; Stein et al., 2020), which is often associated with tropical moisture advection and convective events (Huang et al., 2022; Li et al., 2022a; Lu & Lall, 2016; Saharia et al., 2017a). Beyond this common driver, increased water levels are spatiotemporally differentiated at both large and small scales (Li et al., 2022a) based on atmospheric, watershed, geological, and land cover factors. The results of this study highlight a range of differences in high streamflow characteristics and patterns across the Southeastern United States, albeit with distinct areas defined by regional characteristics. These differences are related to seasonal and annual variability of streamflow peak occurrence and related mechanisms such as precipitation, climatological hydrologic processes (e.g., evapotranspiration, moisture advection), or anthropogenic changes (Kundzewicz et al., 2019; Tramblay et al., 2019; Villarini, 2016).

In general, by the use of multidimensional K-means clustering, four spatial groups can be distinguished, covering: (1): southeast and central Mississippi, Alabama, central Georgia and parts of South Carolina, (2): southwest and north Mississippi, southwest and north Alabama, north and east Georgia and central South Carolina, (3): Florida, parts of the Gulf coast, central and west North Carolina and south Virginia, and (4): southeast North Carolina, the Atlantic coast and parts of the Gulf coast (fig. 15).

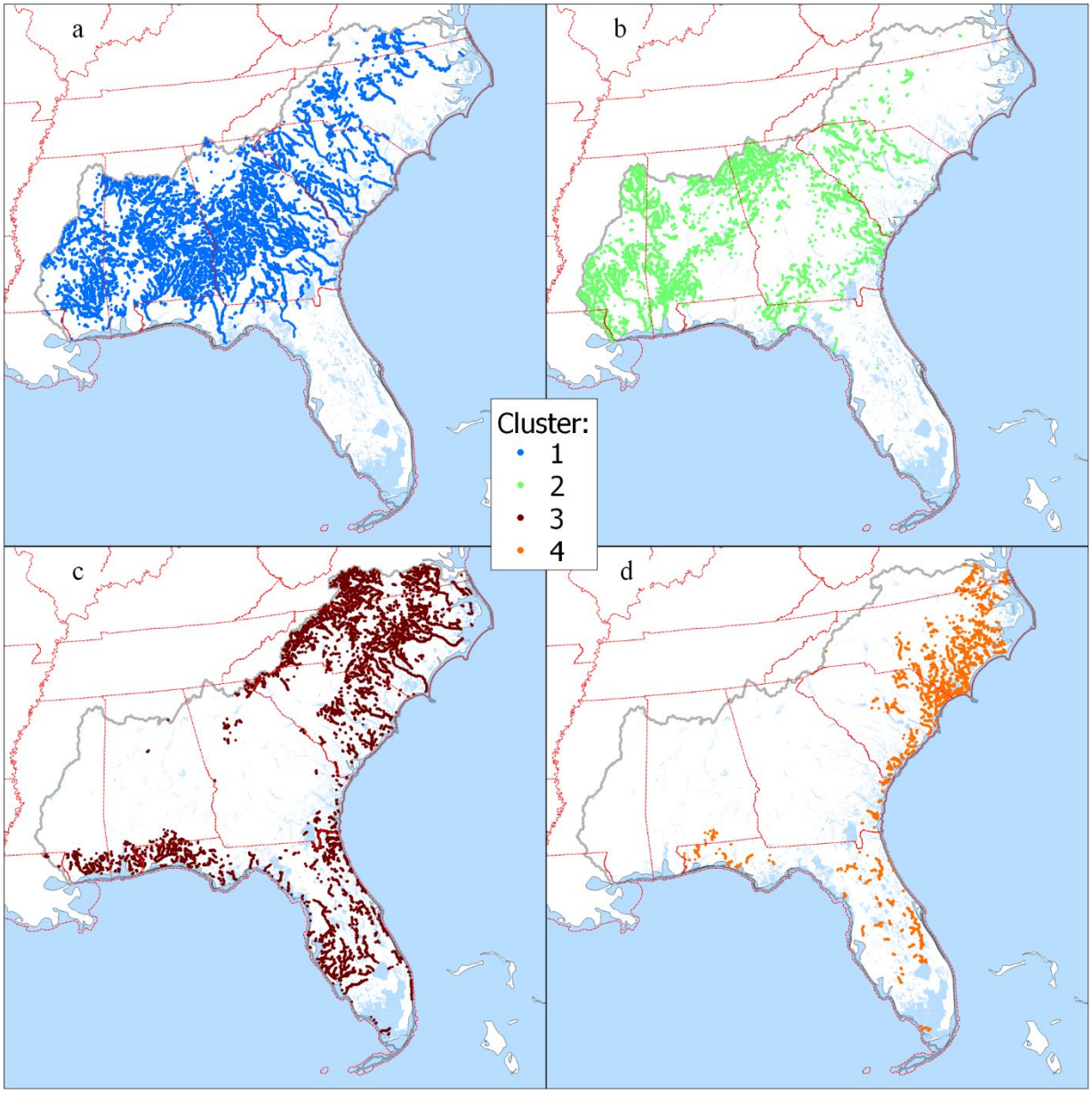

Fig. 15. Flood regionalization over the southeastern United States using multidimensional k-means clustering: cluster 1 (a): Mississippi, Alabama, Georgia, South Carolina; cluster 2 (b): parts of Mississippi, Alabama, Georgia, South Carolina; cluster 3 (c): Florida, North Carolina, Virginia, and Gulf coast; cluster 4 (d): Atlantic coast, parts of Florida and the Gulf coast

The first cluster (fig. 15a) covers major parts of southeast and central Mississippi, Alabama, central Georgia, and parts of South Carolina, where high multiannual SFP occurrence is present (on average $n \approx 125$). A large number of peaks contributes to long total durations (mean

total $t \approx 376$). SFPs have a high contribution to total discharge, with an average cluster $Q_f/Q_t \approx 8\%$. SFPs occur throughout the year, with the highest frequency in December-April and a peak in February and March.

On an annual scale, mainly increasing statistically significant trends in SFP distribution occur only locally in nodes bordering the Walter F. George Reservoir along the Alabama – Georgia border. This highlights potential issues regarding the impact of dams on NWM model output and the specific drivers of streamflow peaks. It must be noted, however, that the NWM retrospective dataset does not include detailed lake/reservoir information such as storage, release, or other operational parameters, but rather a simplified fill and spill technique, implemented for about 5000 reservoirs across the continental US (Cosgrove et al., 2021; Khazaei et al., 2021; Mattern et al., 2021; Rezaeianzadeh et al., 2021; Viterbo et al., 2020). On a short time-scale (hourly to daily) this could severely impact results; however, the monthly and annual aggregations used in this study allow for the treatment of lakes and reservoirs as flow-through units, such that the mass balance (input minus output) is considered zero. As a result, the impact of the lack of dam information on the results is considered minimal.

Detected trends indicate that there has been a change in flood trend directions. Breakpoint analysis conducted by Villarini and Smith (2010) showed that after 1960 there has been a decrease in flooding over eastern Alabama, Georgia and southern Florida. It is most probable that changes here happened in the 1990's, as the trend volatility analysis indicated this as the period with the strongest increasing trends. This agrees with increased flood frequency over the southeastern US found by Ye et al. (2017) for the period 1951-1999 and Paltan et al. (2017) for the period 1979-2010. The highest increases in maximal monthly flows occur in the warm season and into early winter, which is likely related to an increase in observed precipitation over the study area (Marx et al., 2018; Slater & Singer, 2013; Ye et al., 2017), especially due to a change in fall precipitation distribution and in increase in precipitation intensity (Bishop et al., 2019) that translates to increases in flood occurrence (Paltan et al., 2017). The overall increase in maximal flows over the study area in all months is contributing to a decrease in the seasonality of flooding (Ye et al., 2017), but also confirms that changing climate patterns relates to changes in precipitation distribution that then affects flood distribution, as excess precipitation is the main mechanism influencing timing and magnitudes of annual maximal flows in the Southeast US (Berghuijs et al., 2016).

The second cluster (fig. 15b) spans southwest and north Mississippi, north and southwest Alabama, north and east Georgia, and central South Carolina. Although the spatial relation is hard to acknowledge, as the cluster includes nodes in regions like the Appalachian Mountains as well as the coastal plains, this cluster is closely related to the first one, described above. The region is described by the distribution of parameters similar to the first cluster, with a high number of SFPs (mean n=107) and a high share in total outflow (Q_f/Q_t=8%). The main difference between the clusters is the multiannual distribution, where SFP occurred mainly during the 1990-2000 and 2010-2020 periods. In general, a high number of SFP occurrences, with shorter durations and a high share in total discharge, suggest that this cluster may have increased potential for flash flooding. Saharia et al. (2017) identified the Appalachian Mountains as one of the hotspots for flash floods in the United States, and Alipour et al. (2016) found that floods in this area are frequent and usually have similar parameters that could further support flash flood occurrence. In another study, Henderson et al. (2020) found an increased co-occurrence of flash floods with severe convective storms in the area, which could explain the dependence for the southern nodes in this cluster. Few annual trends are observed in this cluster, and winter-spring SFP occurrence from December to April observed in the first and second clusters was also observed by Lecce (2000), Villarini (2016), and Do et al. (2020).

The third cluster (fig. 15c) includes nodes in Florida, the Gulf Coast, central and west North Carolina, as well as south Virginia. The SFP distribution varies over the area, with a mean number of occurrences of n=97 and a mean total duration of t=336 days. The share of SFP volume in total discharge is lower than in the previous clusters, with mean Q_f/Q_t=6%. Regarding seasonal SFP distribution, while South Carolina SFPs occurred mainly between December and April, the North Carolina SFPs occurred throughout the year with significant occurrence during September-October. In the Appalachian piedmont region, increasing annual SFP volume trends are observed with increasing maximal flows for the June-September period and the secondary March flooding period. Gamble (1997) stated that the Carolinas possessed no dominant season in annual flood frequency. In contrast, Villarini (2016) indicated that high flows in the eastern United States tend to occur between October-March, while Lecce (2000) observed uniform monthly distribution of floods in this area. All these statements are true, when considering different parts of the Carolinas within this cluster.

In the southern part of the third cluster, which includes Florida, SFPs occurred throughout the year with maximal occurrence in September-October and a second, lower maxima in March. Around 20-30% of monthly SFP volumes occurred between August and October, while during March, volumes comprised around 15% of annual volumes. These values compare to observations of Lecce (2000) who observed around 54% of annual floods in the August-October period in Florida, with a similar weaker March period. Warm season peaks over Florida were also observed by Alipour et al. (2016), Do et al. (2020) and Villarini (2016). Differences in seasonal distribution are associated with the tropical climate of the Florida region, in which tropical cyclones are responsible for around 40% of high flows (Villarini & Smith, 2010). In the northern Florida nodes, long SFP durations and high shares in total runoff are present, especially in central and eastern areas. Additionally, significant decreasing trends for maximal flows are observed along a latitudinal belt stretching from the Gulf Coast in Alabama through northern Florida to the Atlantic coast of North Carolina. For southern nodes for the same period, maximal flows are increasing, with additional statistically significant increases in annual SFP volumes.

The fourth cluster (fig. 15d) includes nodes along the Atlantic coast, especially in southeast North Carolina, as well as along parts of the Gulf coast. SFPs have the lowest frequency in this cluster (mean of n=10), the shortest total duration (mean of t=53) and a low share in total discharge (mean of Q_f/Qt=2%). Characteristics for nodes in this cluster include strong seasonal occurrences of SFPs, where in September (North Carolina) and October (South Carolina and Virginia), these events contribute over 80% of the total annual SFP volumes. Statistically significant decreasing trends of maximal monthly flows for the June-October period are also present. This might be related to decreasing mean annual precipitation, as observed by Mogollón et al. (2016) or Slater and Villarini (2016). The decreasing tendency could be initiated in the early 1970's, as found by Villarini and Smith (2010). Additionally, Sridhar et al. (2019) observed increasing trends in annual and seasonal extreme daily precipitation over southeastern Virginia, especially in 24- and 48-h precipitation intensity, that could lead to a 50% increase in flood magnitude in the future. This corresponds to an increased trend in stream flashiness found by Mogollón et al. (2016); however, this pattern is not fully recognized in this research, as the coastal area is characterized by the lowest flood frequency, duration, and outflow shares over the study period. On the other hand, the increase in stream flashiness could explain the increasing trends of maximal annual flows, especially since

watersheds in this area gained more urban area, lost forest cover, and had fewer best management practices that could trigger the change in flooding type (Mogollón et al. (2016).

The trend patterns presented above confirm the stated objective of quantifying changes in peak streamflow parameters over the NWM period of record by showing that the majority of nodes indicate no statistically significant trends. This is primarily true for annually aggregated data, as on a monthly scale there are statistically significant regional dependences, especially during the warm season, indicating decreasing SFP distributions in coastal and southern regions and increasing tendencies in the central and northern parts of the study area.

The drivers of these trends relate largely to local environmental conditions, as although large-scale differences are shown to be associated with precipitation, the spatial clusters are related to generalized ecoregions such that differences are reflected in varying regional characteristics. This confirms the primary objective of this study, which is to define the ability of the NWM to identify spatial and temporal patterns of streamflow peaks reflected in local environmental characteristics. Although monthly distributions of SFPs follow the pattern of east-to-west changes, following patterns of precipitation variability, the general regional division of SFPs into clusters shows differences in multiple directions, with southern and eastern nodes showing similarities to each other as opposed to nodes in areas in the northwestern and coastal areas. Although separated into four clusters, the spatial patterns of SFP features continue to be connected to local environmental characteristics. This is consistent with findings from previous research and offer extensive spatial insights into the distribution of SFPs in the southeast US.

The use of the National Water Model (NWM) retrospective dataset greatly increased the spatial coverage of analysis points across the Southeastern US (over 338,000 available nodes, with about 62,000 nodes of 3rd or higher order), which allowed for investigation of streamflow patterns in regions otherwise excluded due to a low density of observed streamflow gauges (520 available points). Additionally, the NWM dataset extends the ability to perform time-series analysis, as continuous temporal data are available from Feb 1979 to Dec 2020 (42 years), compared to non-homogeneous observations from USGS gauges from Jan 1995 to Dec 2018 (24 years). As a result, the NWM retrospective data provides valuable distributed hydrologic information on river stages for water resources management and risk assessment (Hooper et al., 2017).

The mean correlation between NWM simulated data and USGS observations at paired locations gauges located is above r=0.8 and kge>0.5, with a majority of nodes showing above-

average efficiency. Additionally, the performance of the NWM is linked to spatial scale, and increases with size of the basin (Rojas et al., 2020). This indicates good agreement of the model data to real conditions. Some studies suggest the inclusion of at least fourth order nodes in the analysis, due to lower NWM performance in lower order nodes (Dyer et al., 2022; Johnson et al., 2019); however, results from this work indicate that third order nodes are not significantly different from higher order nodes in terms of spatial and temporal patterns. As indicated by Johnson et al. (2019), NWM data-driven approaches might not be highly accurate in terms of point-to-point data values, but perform well in highlighting the regions likely to be at risk of high magnitude streamflow event occurrence. This is further confirmed in this study, where results can be used as spatial and temporal guidelines for regional water management strategies.

Generally, the limitations of model-based approaches in calculation of flow values, as with the case of the NWM, come from limited infiltration quantification abilities, especially noted in semiarid regions (Lahmers et al., 2021), lack of subsurface tile drainage representation (Valayamkunnath et al., 2022), channel routing schemes (Frame et al., 2021) or general simplified hydrologic process representations, and forcing errors (Viterbo et al., 2020). Additionally, it must be noted that in the current version of NWM data (v2.1) only about 5000 reservoirs across the U.S are represented in the model in terms of simplified input-output rules, and the model efficiency in representing real conditions is largely unknown (Viterbo et al., 2020). The impact of reservoir operations on high and low flow peaks is critical; however, with the currently available data, it cannot be assessed in a consistent, distributed manner either by the use of the NWM v2.1 dataset or by observed USGS data. The former due to the indicated model limitations, and the latter due to gauge network density, such that of the 901 recognized dam and reservoir structures located across the Southeastern US, only 73 have a gauge located within a 5 kilometer radius from the dam.

5. Conclusions

The Southeastern United States comprises a variety of physical landscapes and precipitation regimes, leading to multiple streamflow peak (SFP) forming mechanisms and associated distribution patterns. Additionally, flood risk is high for many locations within the region due to high population, minimal topographic relief, and increasing urbanization. In this article, a spatial and temporal assessment of SFP characteristics, including spatial and temporal variability of event frequency, magnitude, and distribution at both annual and monthly scales are

presented. The NWM retrospective data v. 2.1 was used for analysis, which included 61,948 streamflow nodes of Strahler order 3 or higher over the southeast US study area with daily mean flows for the period February 1979 to December 2020. While the patterns of SFPs are complex and highly scale-dependent across the region, an objective method for defining decision threshold was used to define peaks, from which SFP characteristics were defined and analyzed. The overall findings indicate specific regional patterns, defined primarily by climatological rainfall patterns, but with secondary drivers related to regional and local-scale surface and sub-surface conditions and processes.

Results show that the NWM retrospective data are able to differentiate time-related processes leading to SFP formation, and that variations in environmental conditions are reflected in the spatial patterns of SFP distribution. These results agree with other works performed for this region, and confirm the primary objective of the work that the NWM retrospective data are able to identify spatial and temporal patterns of SFP over the southeast US. The secondary objective of quantifying patterns of SFP parameters indicated a lack of statistically significant trends over a majority of annually aggregated series over the study area; however, at a monthly aggregated scale, significant changes were shown to occur during the warm season. These results agree with those from Rodgers et al. (2020), who found mostly no trends in mean monthly streamflow over parts of the southeastern US.

The results of this research provide valuable insight into the complex spatiotemporal patterns of high streamflow peaks over the southeastern US. The identified trends indicate regions where flood management is needed, with increasing importance in coming years. Additionally, the identified spatial and temporal patterns of high flows allow for better adjustment of water management systems, as well as identifying locations where improvement in flood protection infrastructure may be needed. Furthermore, the patterns defined here can be used as a basis for further work focusing on seasonality models, leading to the improvement of future flood forecast systems and methods, as current coarse-scale models providing information over the southeastern US are often insufficient (Do et al., 2020).

Acknowledgements

This research was funded by the National Oceanic and Atmospheric Administration (NOAA), grant number NA19OAR4590411.

Data availability

The data used in this study comes from NOAA National Water Model retrospective dataset in version 2.1 and can be access online at: https://registry.opendata.aws/nwm-archive/ [accessed 4/4/2023].

The objective threshold method used in this study to identify streamflow peaks threshold is available online at: https://github.com/chrisrac/objective_thresholds [accessed 4/4/2023].

CRediT author statement

Conceptualization K.R, J.D.; methodology K.R.; validation K.R., J.D.; formal analysis K.R.; investigation K.R.; resources J.D.; data curation K.R., J.D.; writing—original draft preparation K.R., J.D..; writing—review and editing K.R., J.D.; visualization K.R.; supervision J.D.; project administration J.D.; funding acquisition J.D.; All authors have read and agreed to the published version of the manuscript.

References

Abtew, W., & Trimble, P. (2010). El Niño–Southern Oscillation Link to South Florida Hydrology and Water Management Applications. Water Resources Management, 24(15), 4255–4271. https://doi.org/10.1007/s11269-010-9656-2

Adusumilli, S., Borsa, A. A., Fish, M. A., McMillan, H. K., & Silverii, F. (2019). A Decade of Water Storage Changes Across the Contiguous United States From GPS and Satellite Gravity. Geophysical Research Letters, 46(22), 13006–13015. https://doi.org/10.1029/2019GL085370

Alipour, M. H., Rezakhani, A. T., & Shamsai, A. (2016). Seasonal fractal-scaling of floods in two U.S. water resources regions. Journal of Hydrology, 540, 232–239. https://doi.org/10.1016/j.jhydrol.2016.06.016

Apollonio, C., Balacco, G., Novelli, A., Tarantino, E., & Piccinni, A. F. (2016). Land Use Change Impact on Flooding Areas: The Case Study of Cervaro Basin (Italy). Sustainability, 8(10), Article 10. https://doi.org/10.3390/su8100996

Berghuijs, W. R., Woods, R. A., Hutton, C. J., & Sivapalan, M. (2016). Dominant flood generating mechanisms across the United States: Flood Mechanisms Across the U.S. Geophysical Research Letters, 43(9), 4382–4390. https://doi.org/10.1002/2016GL068070

Bishop, D. A., Williams, A. P., & Seager, R. (2019). Increased Fall Precipitation in the Southeastern United States Driven by Higher-Intensity, Frontal Precipitation. Geophysical Research Letters, 46(14), 8300–8309. https://doi.org/10.1029/2019GL083177

Blodgett, D. L. (2022). National Water Model V2.1 retrospective for selected NWIS gage locations, (1979-2020) [Data set]. U.S. Geological Survey. https://doi.org/10.5066/P9K5BEJG

Burn, D., Whitfield, P. H., Sharif, M. (2016). Identification of changes in floods and flood regimes in Canada using a peaks over threshold approach. Hydrological Processes, 30(18), 3303-3314. https://doi.org/10.1002/hyp.10861

Carlier, C., Wirth, S. B., Cochand, F., Hunkeler, D., & Brunner, P. (2018). Geology controls streamflow dynamics. Journal of Hydrology, 566, 756–769. https://doi.org/10.1016/j.jhydrol.2018.08.069

Casse, C., Gosset, M., Peugeot, C., Pedinotti, V., Boone, A., Tanimoun, B. A., & Decharme, B. (2015). Potential of satellite rainfall products to predict Niger River flood events in Niamey. Atmospheric Research, 163, 162–176. https://doi.org/10.1016/j.atmosres.2015.01.010

Cederstrom, D. J., Boswell, E. H., & Tarver, G. R. (1979). Summary Appraisals of the Nation's Ground-water Resources, South Atlantic-Gulf Region. U.S. Government Printing Office.

Cigler, B. A. (2017). U.S. Floods: The Necessity of Mitigation. State and Local Government Review, 49(2), 127–139. https://doi.org/10.1177/0160323X17731890

Clark, C., Nnaji, G. A., & Huang, W. (2014). Effects of El-Niño and La-Niña Sea Surface Temperature Anomalies on Annual Precipitations and Streamflow Discharges in Southeastern United States. Journal of Coastal Research, 68, 113–120. https://doi.org/10.2112/SI68-015.1

Cook, B. I., Mankin, J. S., Marvel, K., Williams, A. P., Smerdon, J. E., & Anchukaitis, K. J. (2020). Twenty-First Century Drought Projections in the CMIP6 Forcing Scenarios. Earth's Future, 8(6). https://doi.org/10.1029/2019EF001461

Cosgrove, B., Gochis, D., Graziano, T. M., Clark, E. P., & Flowers, T. (2019). The Evolution of NOAA's National Water Model: An Overview of Version 2.1 and Future Operational Plans. AGU Fall Meeting Abstracts, 2019, H51D-01.

Cosgrove, B., Clark, E., Dugger, A., Flowers, T., Gochis, D., Graziano, T., & Ogden, F. (2021). Operational Hydrologic Modeling: Current Status of NOAAs National Water Model and Plans for the Future. 2021, H55U-0971.

Do, H. X., Westra, S., Leonard, M., & Gudmundsson, L. (2020). Global-Scale Prediction of Flood Timing Using Atmospheric Reanalysis. Water Resources Research, 56(1). https://doi.org/10.1029/2019WR024945

Dyer, J.; Mercer, A.; Raczyński, K. (2022). Identifying Spatial Patterns of Hydrologic Drought over the Southeast US Using Retrospective National Water Model Simulations. *Water, 14*, 1525. https://doi.org/10.3390/w14101525

Foks, S. S., Towler, E., Hodson, T. O., Bock, A. R., Dickinson, J. E., Dugger, A. L., Dunne, K. A., Essaid, H. I., Miles, K. J., Over, T. M., Penn, C. A., Russell, A. M., Saxe, S. W., & Simeone, C. E. (2022). Streamflow benchmark locations for hydrologic model evaluation within the conterminous United States (cobalt gages) [Data set]. U.S. Geological Survey. https://doi.org/10.5066/P972P42Z

Frame, J.M., Kratzert, F., Raney, A., Rahman, M., Salas, F.R., and Nearing, G.S.. 2021. " Post-Post-Processing the National Water Model with Long Short-Term Memory Networks for Streamflow Predictions and Model Diagnostics." Journal of the American Water Resources Association 57(6): 885– 905. https://doi.org/10.1111/1752-1688.12964.

Gamble, D. W. (1997). The Relationship Between Drainage Basin Area and Annual Peak-Flood Seasonality in the Southeastern United States. Southeastern Geographer, 37(1), 61–75. https://doi.org/10.1353/sgo.1997.0019

Gangrade, S., Kao, S., Naz, B. S., Rastogi, D., Ashfaq, M., Singh, N., & Preston, B. L. (2018). Sensitivity of Probable Maximum Flood in a Changing Environment. Water Resources Research, 54(6), 3913–3936. https://doi.org/10.1029/2017WR021987

Garousi-Nejad, I., & Tarboton, D. G. (2022). A comparison of National Water Model retrospective analysis snow outputs at snow telemetry sites across the Western United States. Hydrological Processes, 36(1). https://doi.org/10.1002/hyp.14469

Gochis, D., Dugger, A., Yates, D., Sampson, K., Barlage, M., Pan, L., Zhang, Y., McCreight, J., RafieeiNasab, A., Karsten, L., Fitzgerald, K., Mills, J., Read, L., Gaydos, A., Cabell, R., Grim, J., Towler, E., Cosgrove, B., Clark, E., … Ogden, F. (2018). Multi-variate evaluation of the NOAA National Water Model. [online: https://ral.ucar.edu/sites/default/files/public/Multi-variate%20evaluation%20of%20the%20NOAA%20National%20Water%20Model_Dec_2018.pdf]

Henderson, J., Nielsen, E. R., Herman, G. R., & Schumacher, R. S. (2020). A Hazard Multiple: Overlapping Tornado and Flash Flood Warnings in a National Weather Service Forecast Office in the Southeastern United States. Weather and Forecasting, 35(4), 1459–1481. https://doi.org/10.1175/WAF-D-19-0216.1

Hooper, Richard P.; Nearing, Grey; and Condon, Laura S. (2017). Using the National Water Model as a Hypothesis-Testing Tool. Open Water Journal, 4(2), Article 3

Huang, H., Fischella, M. R., Liu, Y., Ban, Z., Fayne, J. V., Li, D., Cavanaugh, K. C., & Lettenmaier, D. P. (2022). Changes in Mechanisms and Characteristics of Western U.S. Floods Over the Last Sixty Years. Geophysical Research Letters, 49(3). https://doi.org/10.1029/2021GL097022

Hussain, Md., & Mahmud, I. (2019). pyMannKendall: A python package for non parametric Mann Kendall family of trend tests. Journal of Open Source Software, 4(39), 1556. https://doi.org/10.21105/joss.01556

Jevrejeva, S., Jackson, L. P., Grinsted, A., Lincke, D., & Marzeion, B. (2018). Flood damage costs under the sea level rise with warming of 1.5 °C and 2 °C. Environmental Research Letters, 13(7), 074014. https://doi.org/10.1088/1748-9326/aacc76

Johnson, L. E., & Kim, J. (2019). NATIONAL WATER MODEL RETROSPECTIVE SIMULATION ASSESSMENT [online: https://psl.noaa.gov/aqpi/users/meeting1/AQPI_TribHydro_Retro_23Jan20.pdf]

Johnson, J. M., Munasinghe, D., Eyelade, D., and Cohen, S. (2019). An integrated evaluation of the National Water Model (NWM)–Height Above Nearest Drainage (HAND) flood mapping methodology, Nat. Hazards Earth Syst. Sci., 19, 2405–2420, https://doi.org/10.5194/nhess-19-2405-2019

Joshi, N., Kalra, A., & Lamb, K. W. (2020). Land–Ocean–Atmosphere Influences on Groundwater Variability in the South Atlantic–Gulf Region. Hydrology, 7(4), 71. https://doi.org/10.3390/hydrology7040071

Kazakis, N., Kougias, I., & Patsialis, T. (2015). Assessment of flood hazard areas at a regional scale using an index-based approach and Analytical Hierarchy Process: Application in Rhodope–Evros region, Greece. Science of The Total Environment, 538, 555–563. https://doi.org/10.1016/j.scitotenv.2015.08.055

Keellings, D., & Engström, J. (2019). The Future of Drought in the Southeastern U.S.: Projections from Downscaled CMIP5 Models. Water, 11(2), 259. https://doi.org/10.3390/w11020259

Khazaei, B., Read, L. K., Casali, M., Sampson, K. M., & Yates, D. (2021). Improvement of Lake and Reservoir Parameterization in the NOAA National Water Model. 552–560. https://doi.org/10.1061/9780784483466.050

Komsta, Ł. (2006). Processing Data for Outliers. R News, 6(2), 10-13.

Kundzewicz, Szwed, & Pińskwar. (2019). Climate Variability and Floods—A global Review. Water, 11(7), 1399. https://doi.org/10.3390/w11071399

Lahmers, T. M., and Coauthors, 2021: Evaluation of NOAA National Water Model Parameter Calibration in Semiarid Environments Prone to Channel Infiltration. J. Hydrometeor., 22, 2939–2969, https://doi.org/10.1175/JHM-D-20-0198.1

Lecce, S. A. (2000). Spatial variations in the timing of annual floods in the southeastern United States. Journal of Hydrology, 235(3–4), 151–169. https://doi.org/10.1016/S0022-1694(00)00273-0

Li, Z., Gao, S., Chen, M., Gourley, J. J., & Hong, Y. (2022a). Spatiotemporal characteristics of US floods: Current status and forecast under a future warmer climate. Earth's Future. https://doi.org/10.1029/2022EF002700

Li, Z., Gao, S., Chen, M., Gourley, J. J., Liu, C., Prein, A. F., & Hong, Y. (2022b). The conterminous United States are projected to become more prone to flash floods in a high-end emissions scenario. Communications Earth & Environment, 3(1), 86. https://doi.org/10.1038/s43247-022-00409-6

Lu, M., & Lall, U. (2016). Tropical Moisture Exports, Extreme Precipitation and Floods in Northeast US [Preprint]. Hydrometeorology/Theory development. https://doi.org/10.5194/hess-2016-403

Marx, A., Kumar, R., Thober, S., Rakovec, O., Wanders, N., Zink, M., Wood, E. F., Pan, M., Sheffield, J., & Samaniego, L. (2018). Climate change alters low flows in Europe under global warming of 1.5, 2, and 3 °C. Hydrology and Earth System Sciences, 22(2), 1017–1032. https://doi.org/10.5194/hess-22-1017-2018

Mattern, D., Frazier, N., Wlostowski, A., Halgren, J. S., Rezaeianzadeh, M., Flowers, T., & Aggett, G. (2021). Reservoir Integration into Dendritic Inland Hydraulic Routing for National Water Model V3.0. 2021, H45N-1340.

Mogollón, B., Frimpong, E. A., Hoegh, A. B., & Angermeier, P. L. (2016). Recent Changes in Stream Flashiness and Flooding, and Effects of Flood Management in North Carolina and Virginia. JAWRA Journal of the American Water Resources Association, 52(3), 561–577. https://doi.org/10.1111/1752-1688.12408

Mourtzinis, S., Ortiz, B. V., & Damianidis, D. (2016). Climate Change and ENSO Effects on Southeastern US Climate Patterns and Maize Yield. Scientific Reports, 6(1), 29777. https://doi.org/10.1038/srep29777

Nakamura, J., Lall, U., Kushnir, Y., Robertson, A. W., & Seager, R. (2013). Dynamical Structure of Extreme Floods in the U.S. Midwest and the United Kingdom. Journal of Hydrometeorology, 14(2), 485–504. https://doi.org/10.1175/JHM-D-12-059.1

Niyogi, D., Lei, M., Kishtawal, C., Schmid, P., & Shepherd, M. (2017). Urbanization Impacts on the Summer Heavy Rainfall Climatology over the Eastern United States. Earth Interactions, 21(5), 1–17. https://doi.org/10.1175/EI-D-15-0045.1

NOAA National Water Model CONUS Retrospective Dataset was accessed on 5/2022 from https://registry.opendata.aws/nwm-archive.

Oudin, L., Salavati, B., Furusho-Percot, C., Ribstein, P., & Saadi, M. (2018). Hydrological impacts of urbanization at the catchment scale. Journal of Hydrology, 559, 774–786. https://doi.org/10.1016/j.jhydrol.2018.02.064

Paltan, H., Waliser, D., Lim, W. H., Guan, B., Yamazaki, D., Pant, R., & Dadson, S. (2017). Global Floods and Water Availability Driven by Atmospheric Rivers: Global Hydrology and ARs. Geophysical Research Letters, 44(20), 10,387-10,395. https://doi.org/10.1002/2017GL074882

Prime, T., Brown, J. M., & Plater, A. J. (2016). Flood inundation uncertainty: The case of a 0.5% annual probability flood event. Environmental Science & Policy, 59, 1–9. https://doi.org/10.1016/j.envsci.2016.01.018

Raczyński, K., & Dyer, J. (2022). Development of an Objective Low Flow Identification Method Using Breakpoint Analysis. Water, 14(14), Article 14. https://doi.org/10.3390/w14142212

Rahman, M. A., Zhang, Y., Ghazvinian, M., Fernando, N., Schoenbaechler, C., & Gan, Y. (2022). Assessment of Relative Accuracy of TxRR and NWM in Simulating Streamflow for a Cluster of Watersheds along the south Texas Coast [Preprint]. ENGINEERING. https://doi.org/10.20944/preprints202210.0415.v1

Rezaeianzadeh, M., Mattern, D., Frazier, N., Khazaei, B., Yates, D., Sampson, K., Dugger, A., Cosgrove, B., Read, L., Cui, Z., Liu, Y., Johnson, D., Flowers, T., & Aggett, G. (2021). Active Water Management within the National Water Model V3.0: Assimilation of Reservoir Outflow and Glacier Dammed Lake Releases. 2021, H45O-1351.

Rodgers, K., Roland, V., Hoos, A., Crowley-Ornelas, E., & Knight, R. (2020). An Analysis of Streamflow Trends in the Southern and Southeastern US from 1950–2015. Water, 12(12), 3345. MDPI AG. Retrieved from http://dx.doi.org/10.3390/w12123345

Rojas, M., Quintero, F., and Krajewski, W.F. (2020). Performance of the National Water Model in Iowa Using Independent Observations. JAWRA Journal of the American Water Resources Association 56 (4): 568– 585. https://doi.org/10.1111/1752-1688.12820

Sagarika, S., Kalra, A., & Ahmad, S. (2015). Interconnections between oceanic–atmospheric indices and variability in the U.S. streamflow. Journal of Hydrology, 525, 724–736. https://doi.org/10.1016/j.jhydrol.2015.04.020

Saharia, M., Kirstetter, P.-E., Vergara, H., Gourley, J. J., & Hong, Y. (2017a). Characterization of floods in the United States. Journal of Hydrology, 548, 524–535. https://doi.org/10.1016/j.jhydrol.2017.03.010

Saharia, M., Kirstetter, P.-E., Vergara, H., Gourley, J. J., Hong, Y., & Giroud, M. (2017b). Mapping Flash Flood Severity in the United States. Journal of Hydrometeorology, 18(2), 397–411. https://doi.org/10.1175/JHM-D-16-0082.1

Sinaga, K. P., & Yang, M.-S. (2020). Unsupervised K-Means Clustering Algorithm. IEEE Access, 8, 80716–80727. https://doi.org/10.1109/ACCESS.2020.2988796

Slater, L. J., & Singer, M. B. (2013). Imprint of climate and climate change in alluvial riverbeds: Continental United States, 1950-2011. Geology, 41(5), 595–598. https://doi.org/10.1130/G34070.1

Slater, L. J., & Villarini, G. (2016). Recent trends in U.S. flood risk. Geophysical Research Letters, 43(24). https://doi.org/10.1002/2016GL071199

Sridhar, V., Modi, P., Billah, M. M., Valayamkunnath, P., & Goodall, J. L. (2019). Precipitation Extremes and Flood Frequency in a Changing Climate in Southeastern Virginia. JAWRA Journal of the American Water Resources Association, 55(4), 780–799. https://doi.org/10.1111/1752-1688.12752

Stein, L., Pianosi, F., & Woods, R. (2020). Event-based classification for global study of river flood generating processes. Hydrological Processes, 34(7), 1514–1529. https://doi.org/10.1002/hyp.13678

Towler, E., Foks, S. S., Dugger, A. L., Dickinson, J. E., Essaid, H. I., Gochis, D., Viger, R. J., & Zhang, Y. (2022). Benchmarking High-Resolution, Hydrologic Performance of Long-Term Retrospectives in the United States [Preprint]. Rivers and Lakes/Modelling approaches. https://doi.org/10.5194/hess-2022-276

Tramblay, Y., Mimeau, L., Neppel, L., Vinet, F., & Sauquet, E. (2019). Detection and attribution of flood trends in Mediterranean basins. Hydrology and Earth System Sciences, 23(11), 4419–4431. https://doi.org/10.5194/hess-23-4419-2019

Valayamkunnath, P., Gochis, D. J., Chen, F., Barlage, M., & Franz, K. J. (2022). Modeling the hydrologic influence of subsurface tile drainage using the National Water Model. Water Resources Research, 58, e2021WR031242. https://doi.org/10.1029/2021WR031242

Villarini, G. (2016). On the seasonality of flooding across the continental United States. Advances in Water Resources, 87, 80–91. https://doi.org/10.1016/j.advwatres.2015.11.009

Villarini, G., & Smith, J. A. (2010). Flood peak distributions for the eastern United States: EASTERN UNITED STATES FLOODS. Water Resources Research, 46(6). https://doi.org/10.1029/2009WR008395

Viterbo, F., Mahoney, K., Read, L., Salas, F., Bates, B., Elliott, J., Cosgrove, B., Dugger, A., Gochis, D., & Cifelli, R. (2020). A Multiscale, Hydrometeorological Forecast Evaluation of National Water Model Forecasts of the May 2018 Ellicott City, Maryland, Flood, Journal of Hydrometeorology, 21(3), 475-499. doi: https://doi.org/10.1175/JHM-D-19-0125.1

Viterbo, F., Read, L., Nowak, K., Wood, A. W., Gochis, D., Cifelli, R., & Hughes, M. (2020). General Assessment of the Operational Utility of National Water Model Reservoir Inflows for the Bureau of Reclamation Facilities. Water, 12(10), 2897. http://dx.doi.org/10.3390/w12102897

Vogler, J. B., & Vukomanovic, J. (2021). Trends in United States Human Footprint Revealed by New Spatial Metrics of Urbanization and Per Capita Land Change. Sustainability, 13(22), 12852. https://doi.org/10.3390/su132212852

Wald, A., & Wolfowitz, J. (1942). An exact test for randomness in the non-parametric case, based on serial correlation. Annual Mathematical Statistics, 14, 378-388

Wan, T., Covert, B. H., Kroll, C. N., & Ferguson, C. R. (2022). An Assessment of the National Water Model's Ability to Reproduce Drought Series in the Northeastern United States. Journal of Hydrometeorology, 23(12), 1929–1943. https://doi.org/10.1175/JHM-D-21-0226.1

Wang, F., Shao, W., Yu, H., Kan, G., He, X., Zhang, D., Ren, M., & Wang, G. (2020). Re-evaluation of the Power of the Mann-Kendall Test for Detecting Monotonic Trends in Hydrometeorological Time Series. Frontiers in Earth Science, 8. https://www.frontiersin.org/articles/10.3389/feart.2020.00014

Ye, S., Li, H.-Y., Leung, L. R., Guo, J., Ran, Q., Demissie, Y., & Sivapalan, M. (2017). Understanding Flood Seasonality and Its Temporal Shifts within the Contiguous United States. Journal of Hydrometeorology, 18(7), 1997–2009. https://doi.org/10.1175/JHM-D-16-0207.1

Yue, S., Pilon, P., & Cavadias, G. (2002). Power of the Mann–Kendall and Spearman's rho tests for detecting monotonic trends in hydrological series. Journal of Hydrology, 259(1-4), 254–271. https://doi.org/10.1016/s0022-1694(01)00594-7

Zope, P. E., Eldho, T. I., & Jothiprakash, V. (2016). Impacts of land use–land cover change and urbanization on flooding: A case study of Oshiwara River Basin in Mumbai, India. CATENA, 145, 142–154. https://doi.org/10.1016/j.catena.2016.06.009

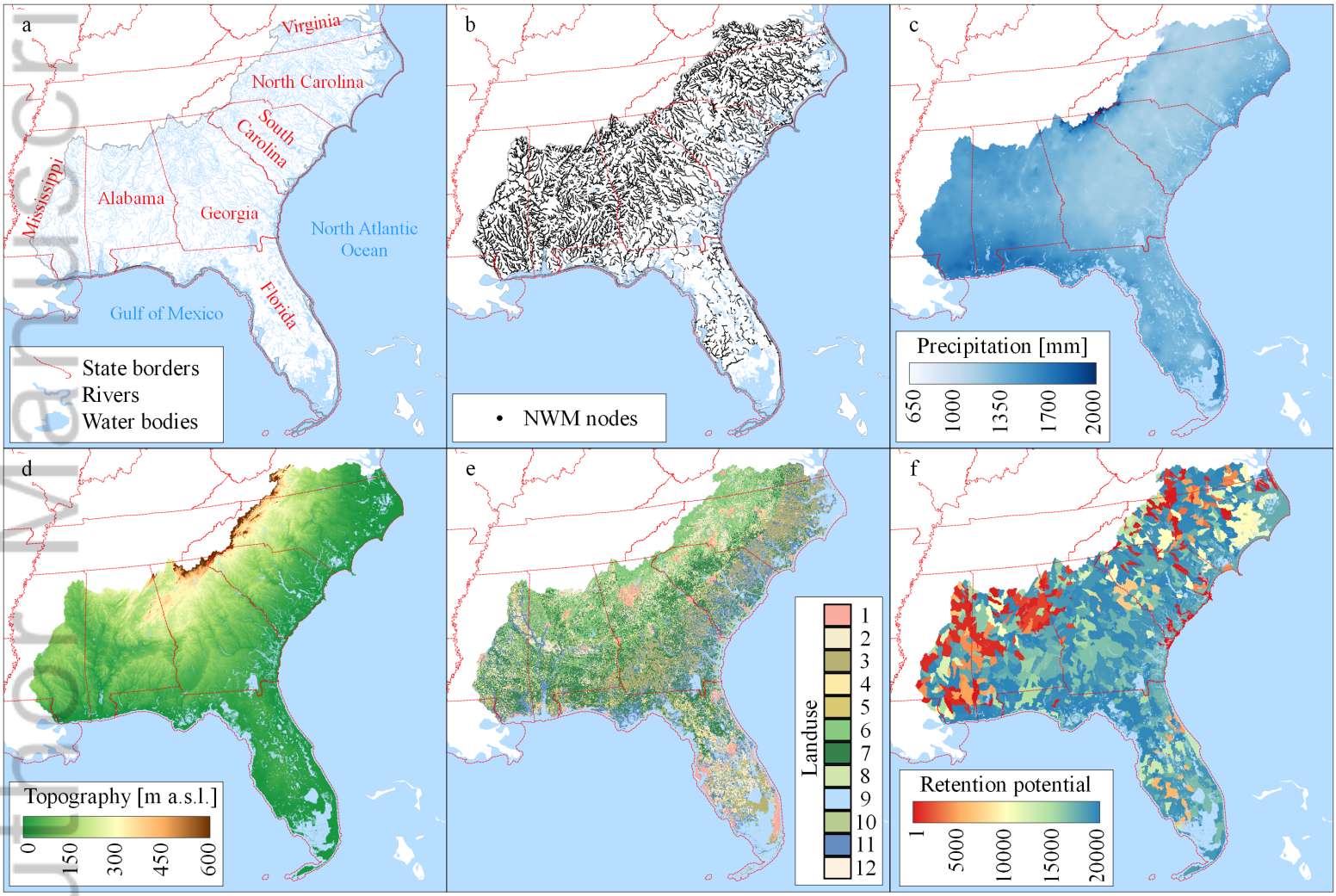

fig1.tiff

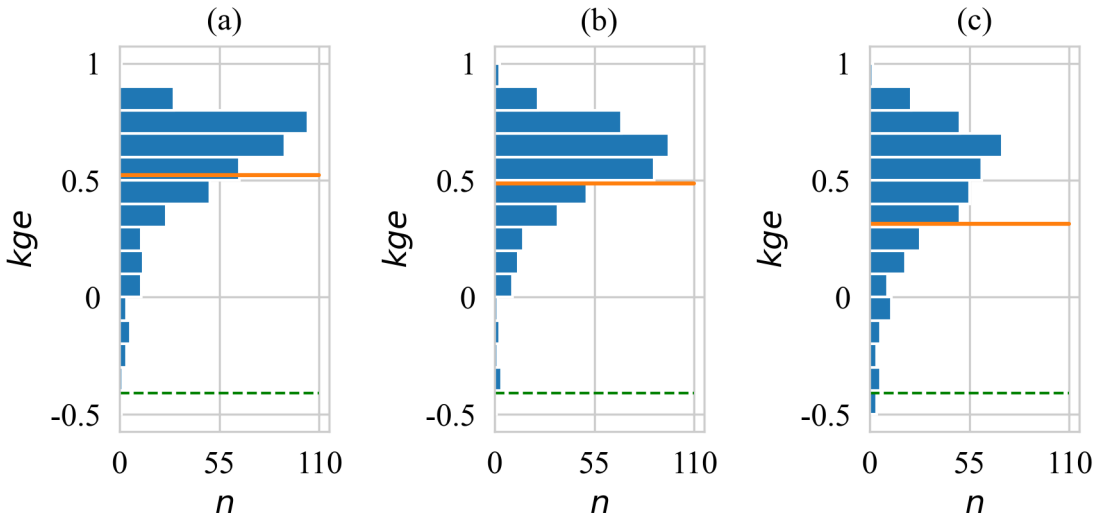

fig2.tiff

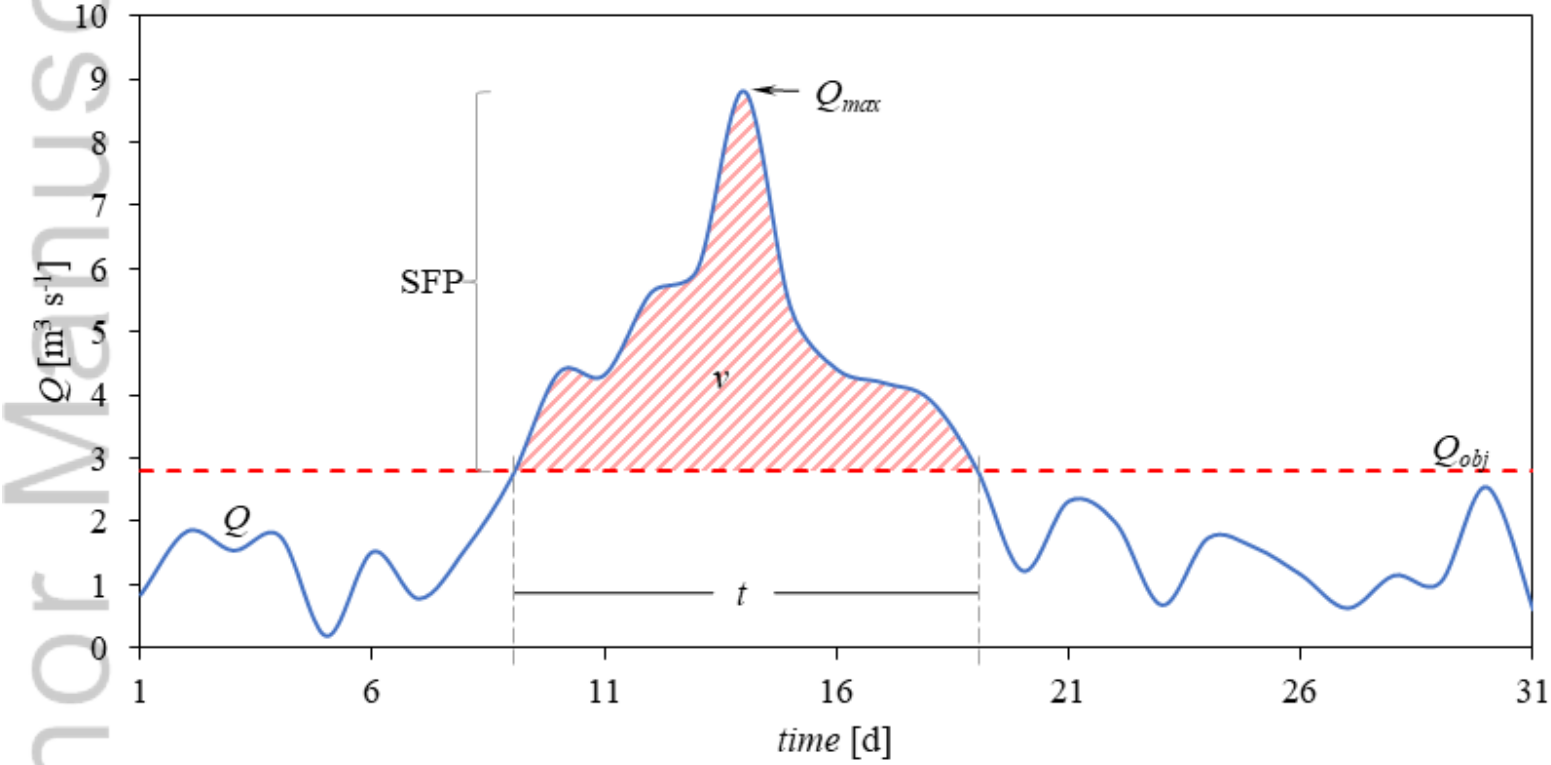

fig3.tif

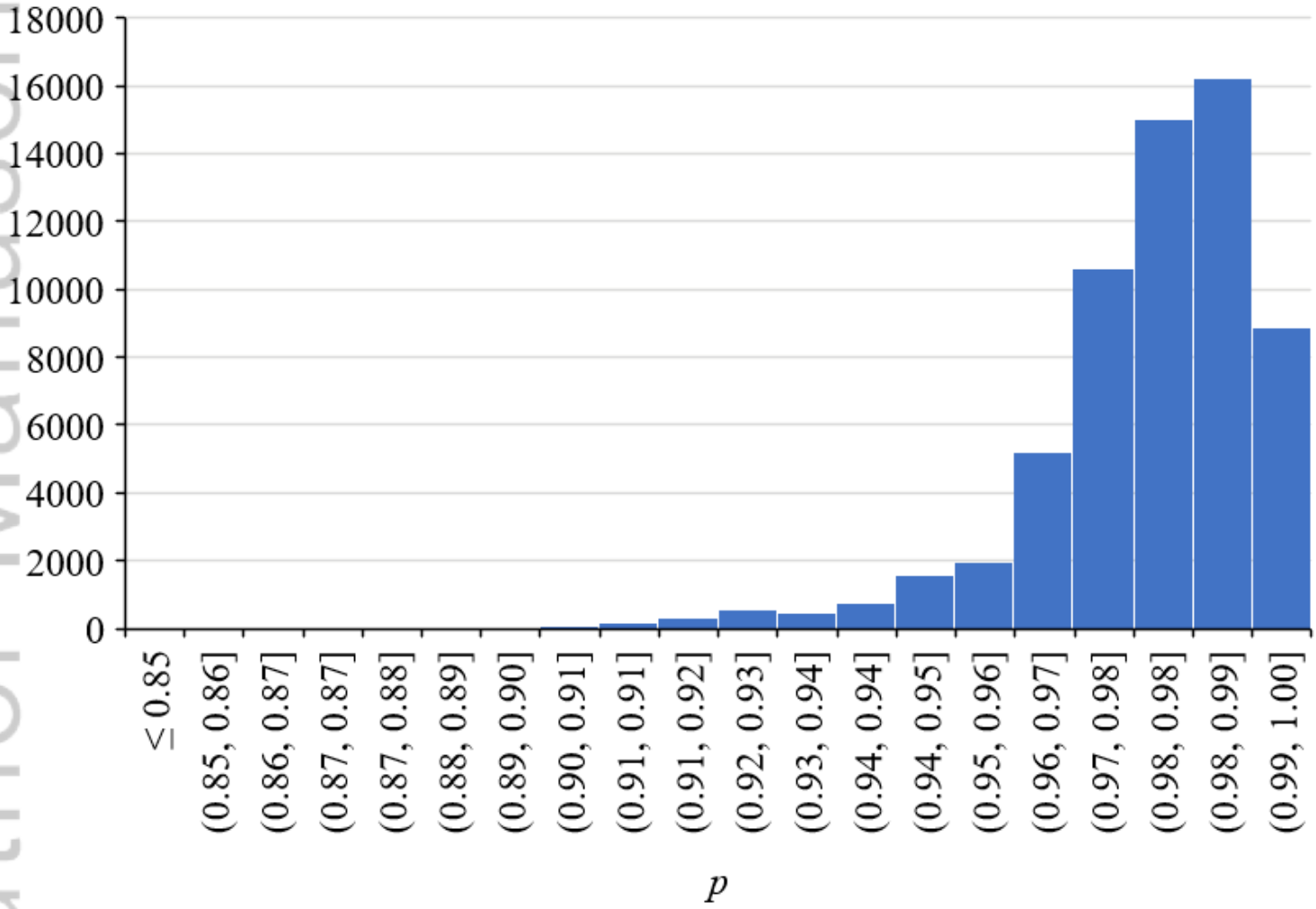

fig4.png

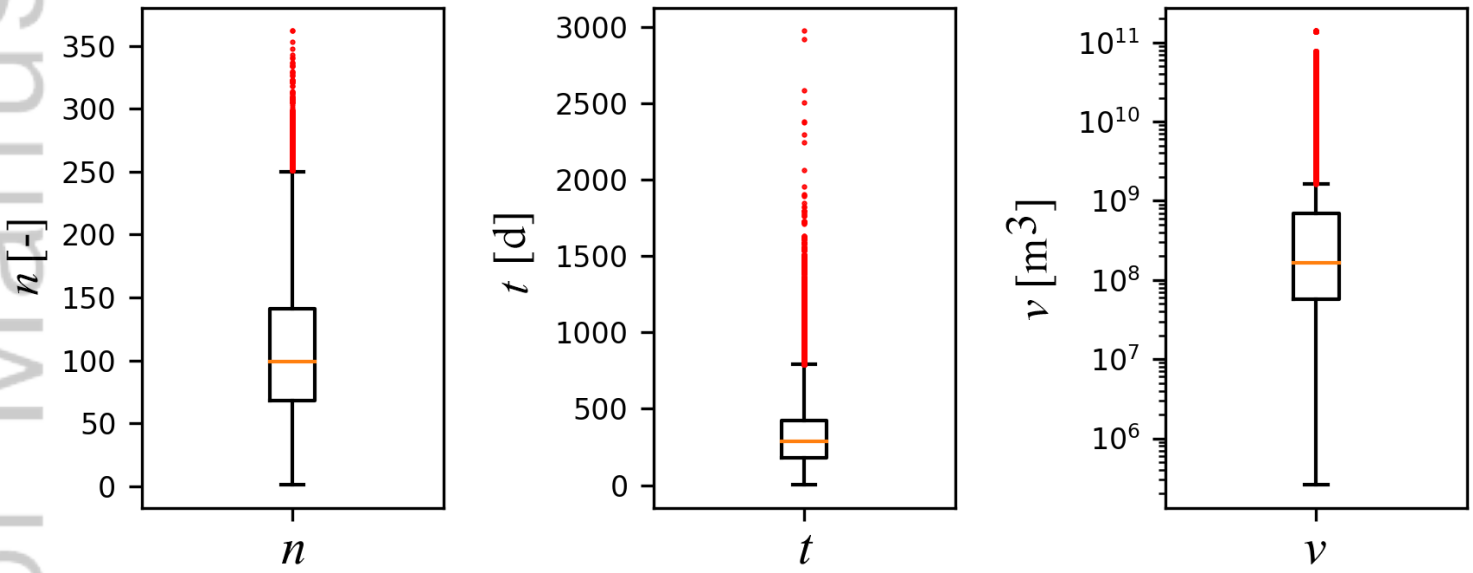

fig5.png

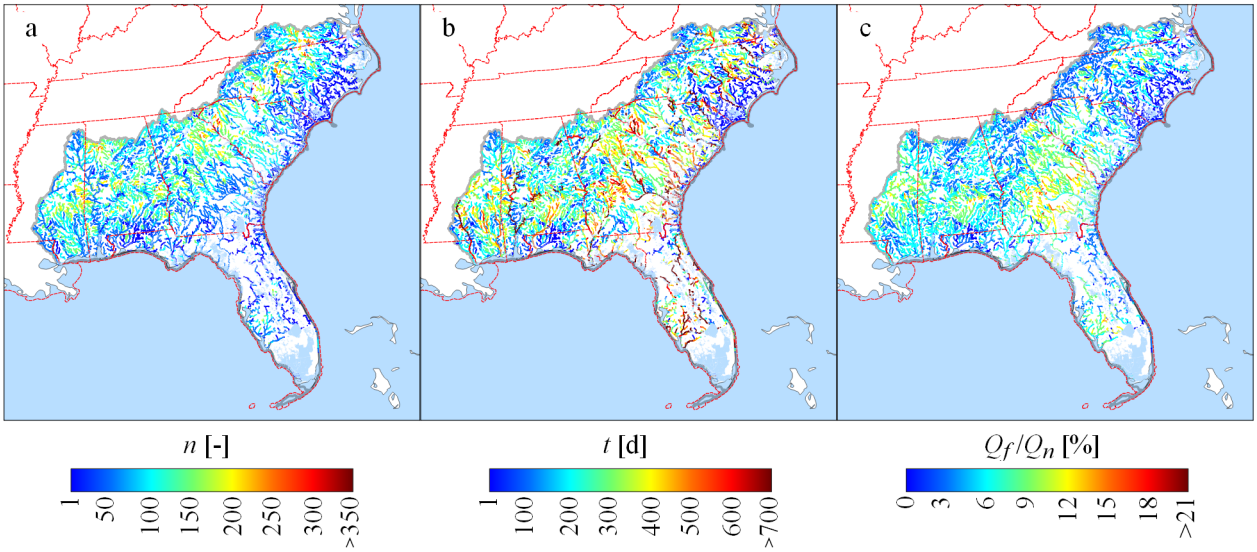

fig6.tiff

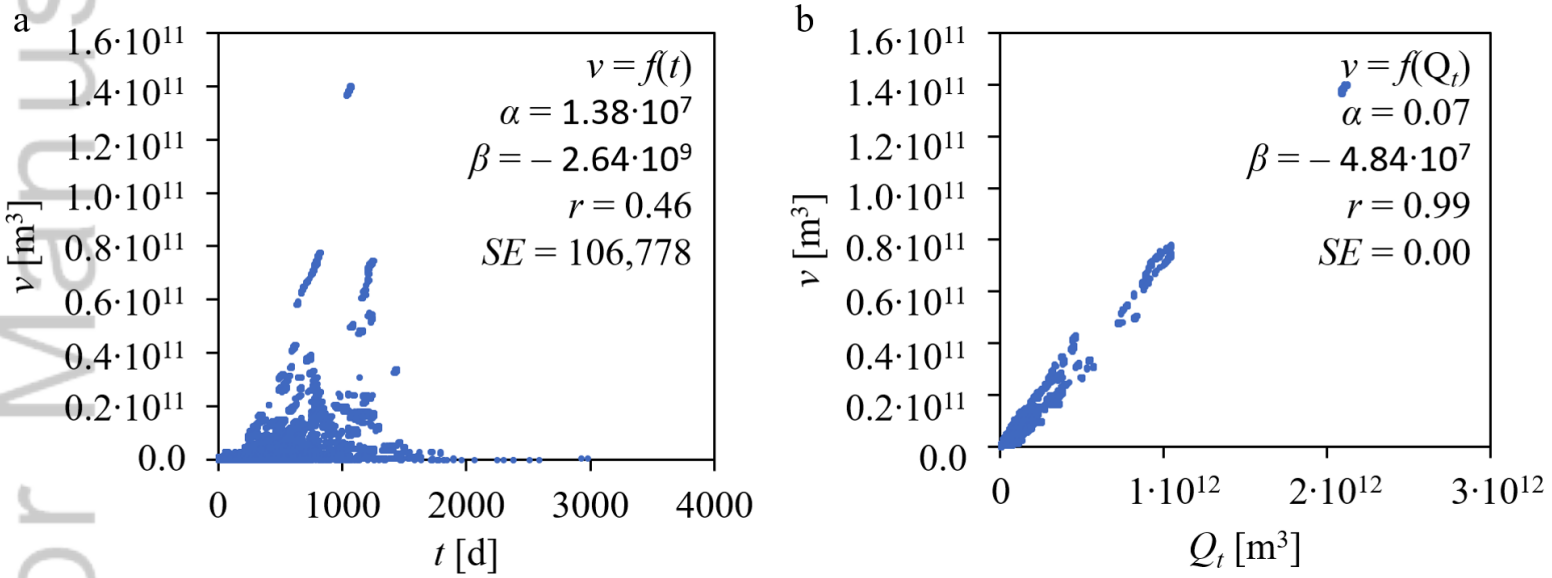

fig7.tif

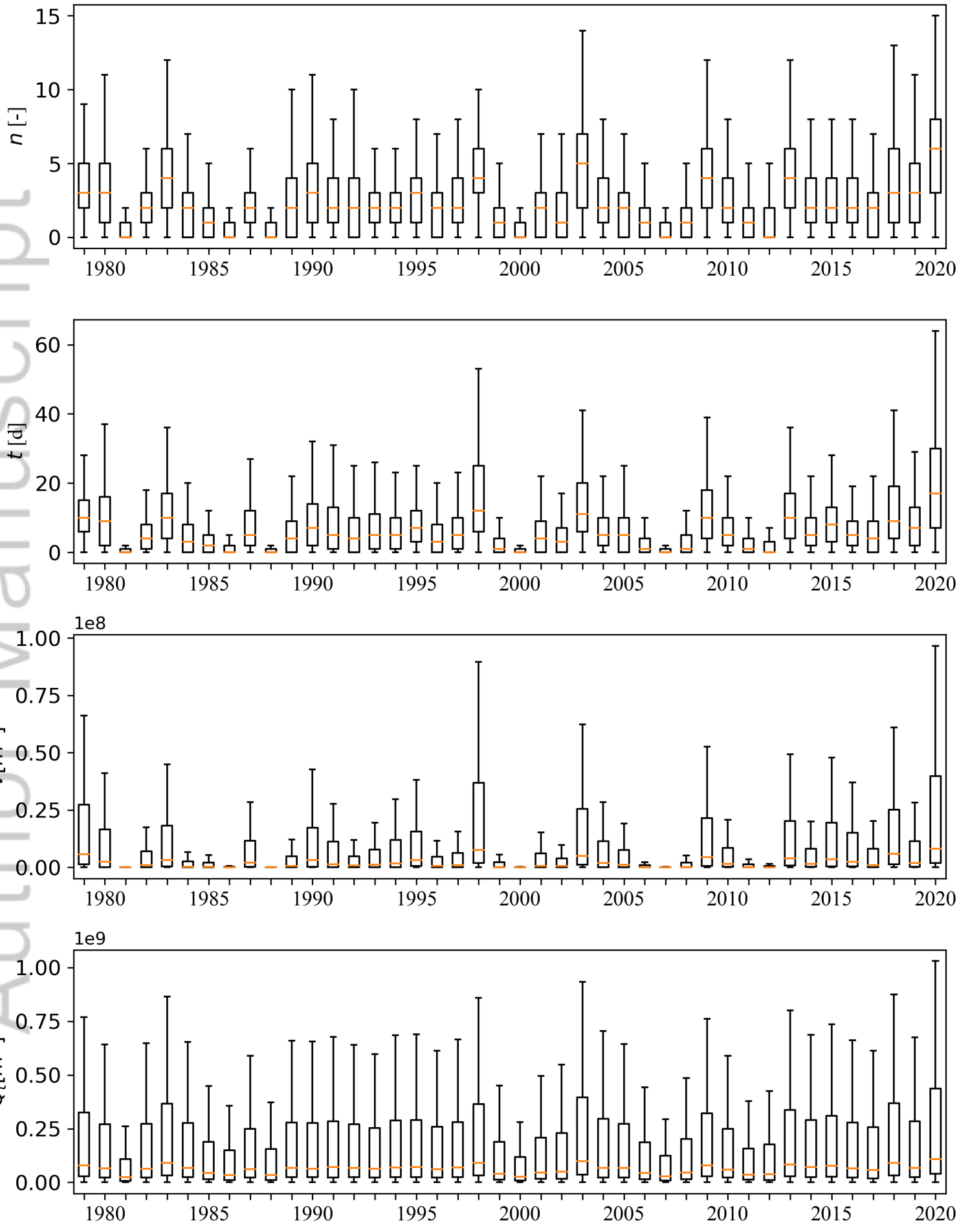

fig8.png

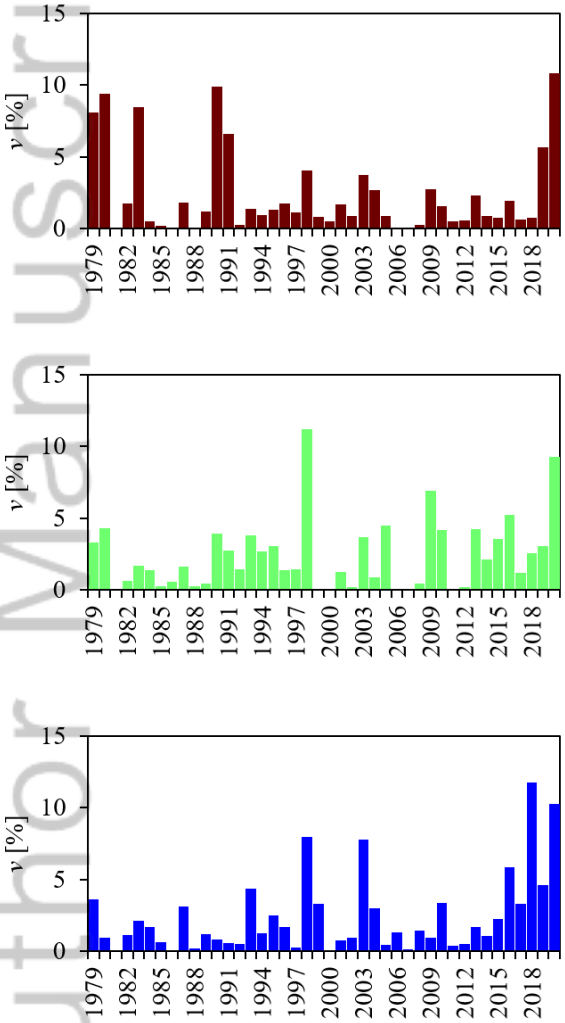

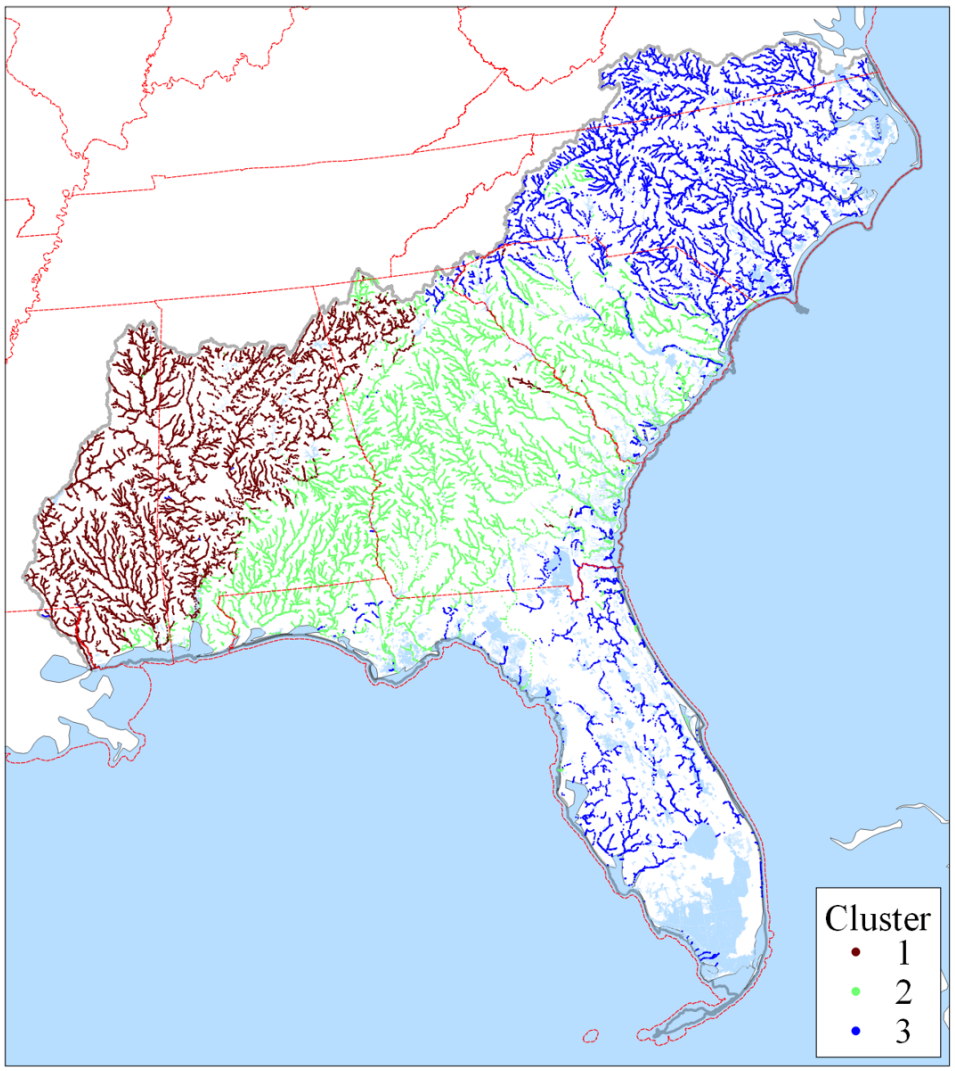

fig9.TIF

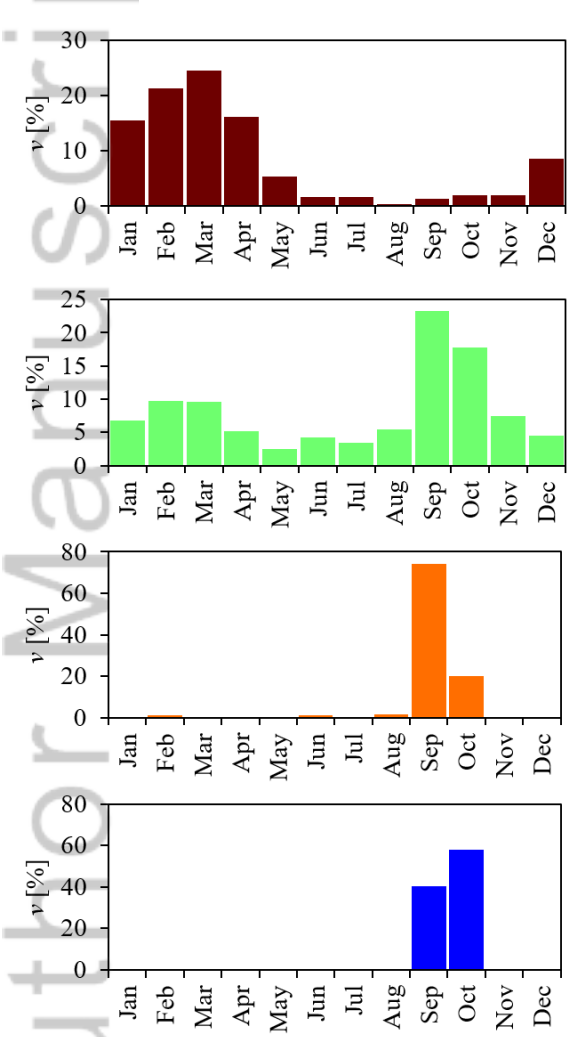

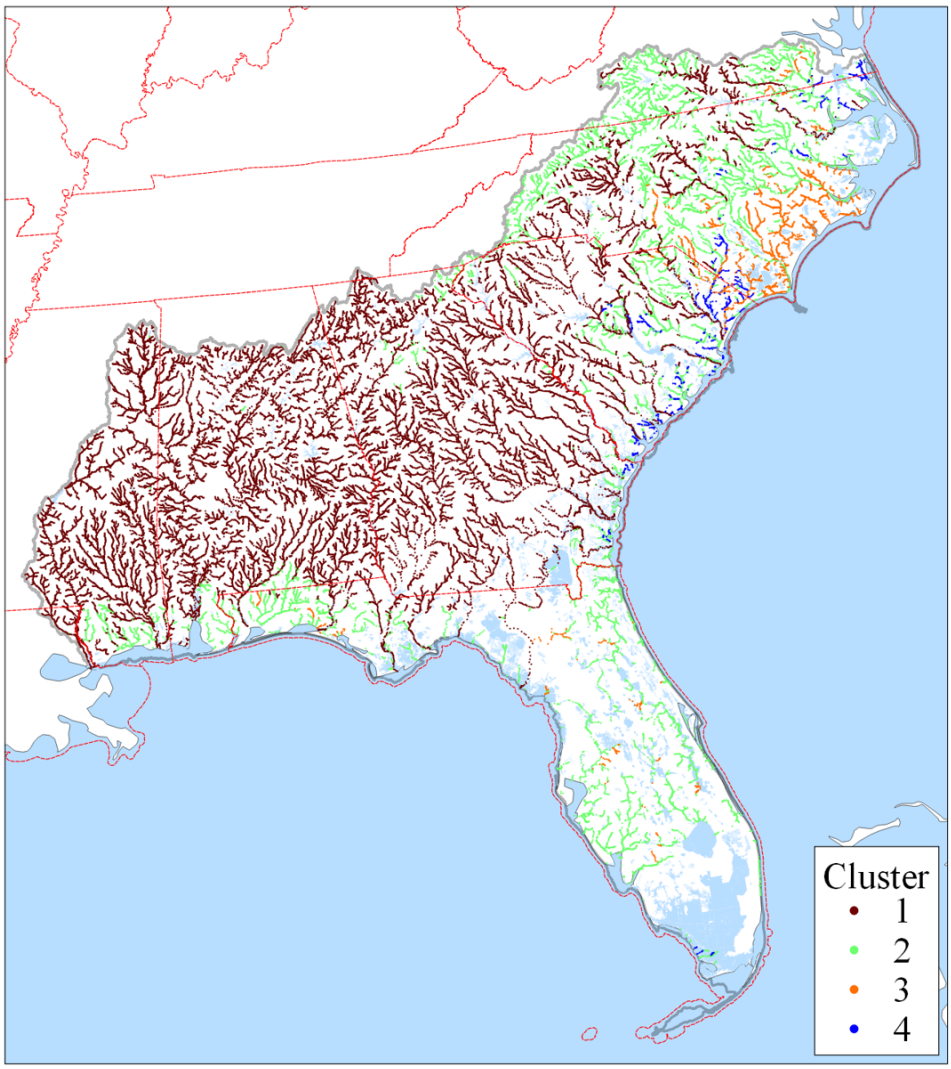

fig10.TIF

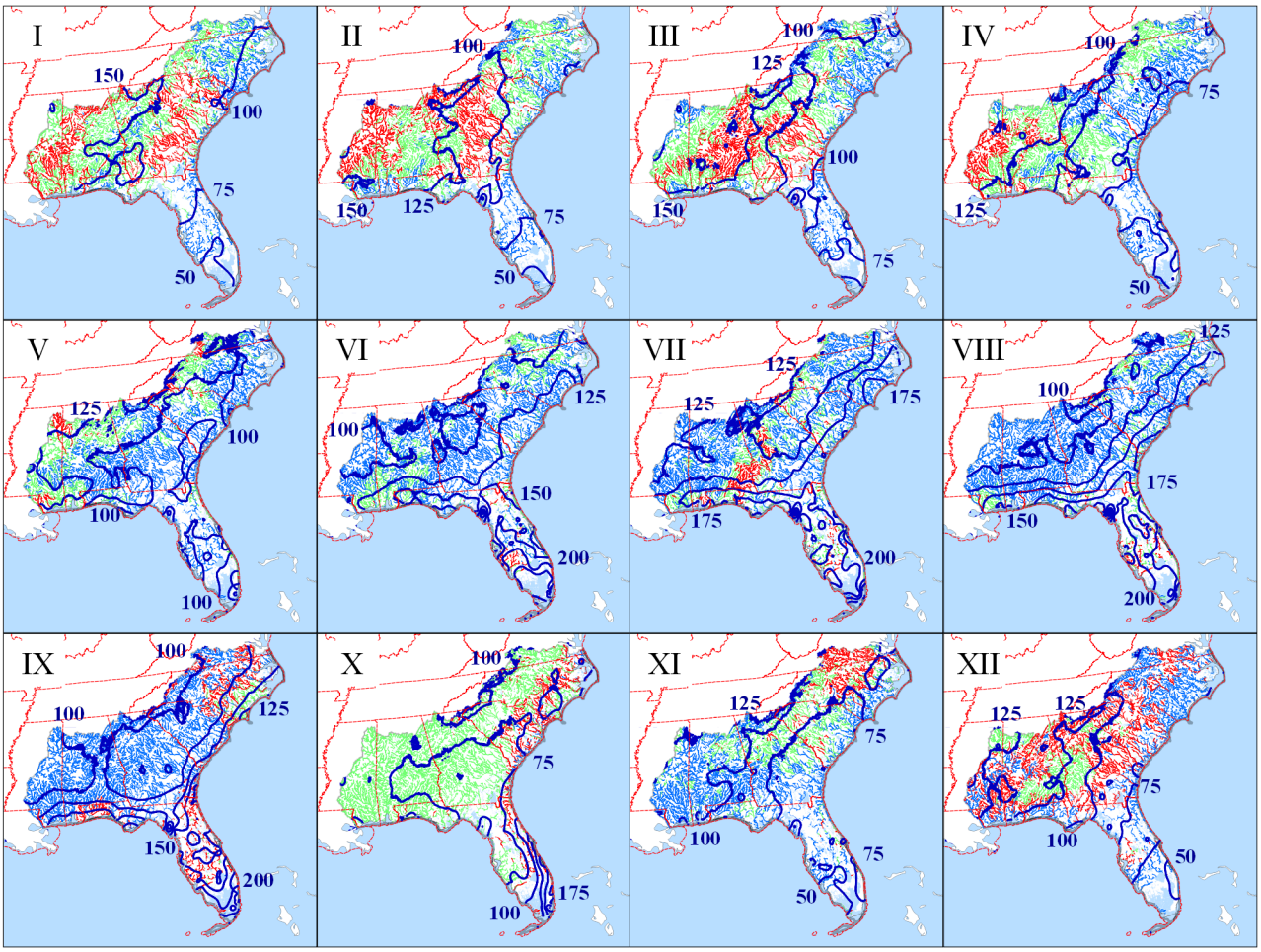

fig11.tiff

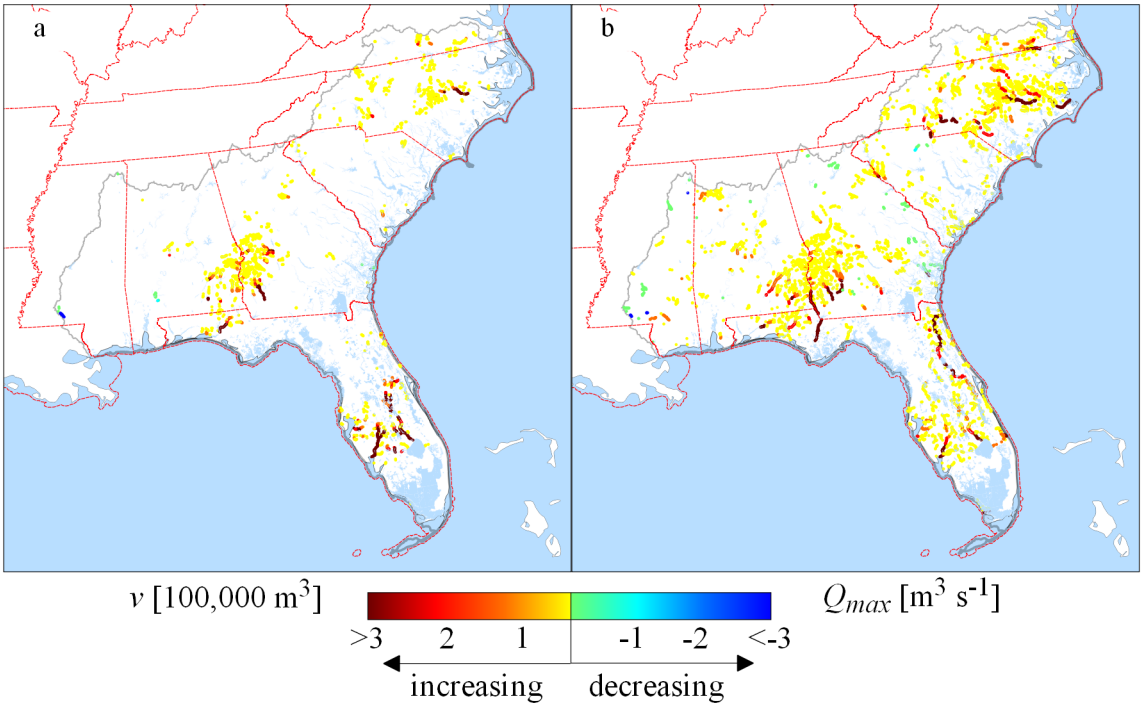

fig12.tiff

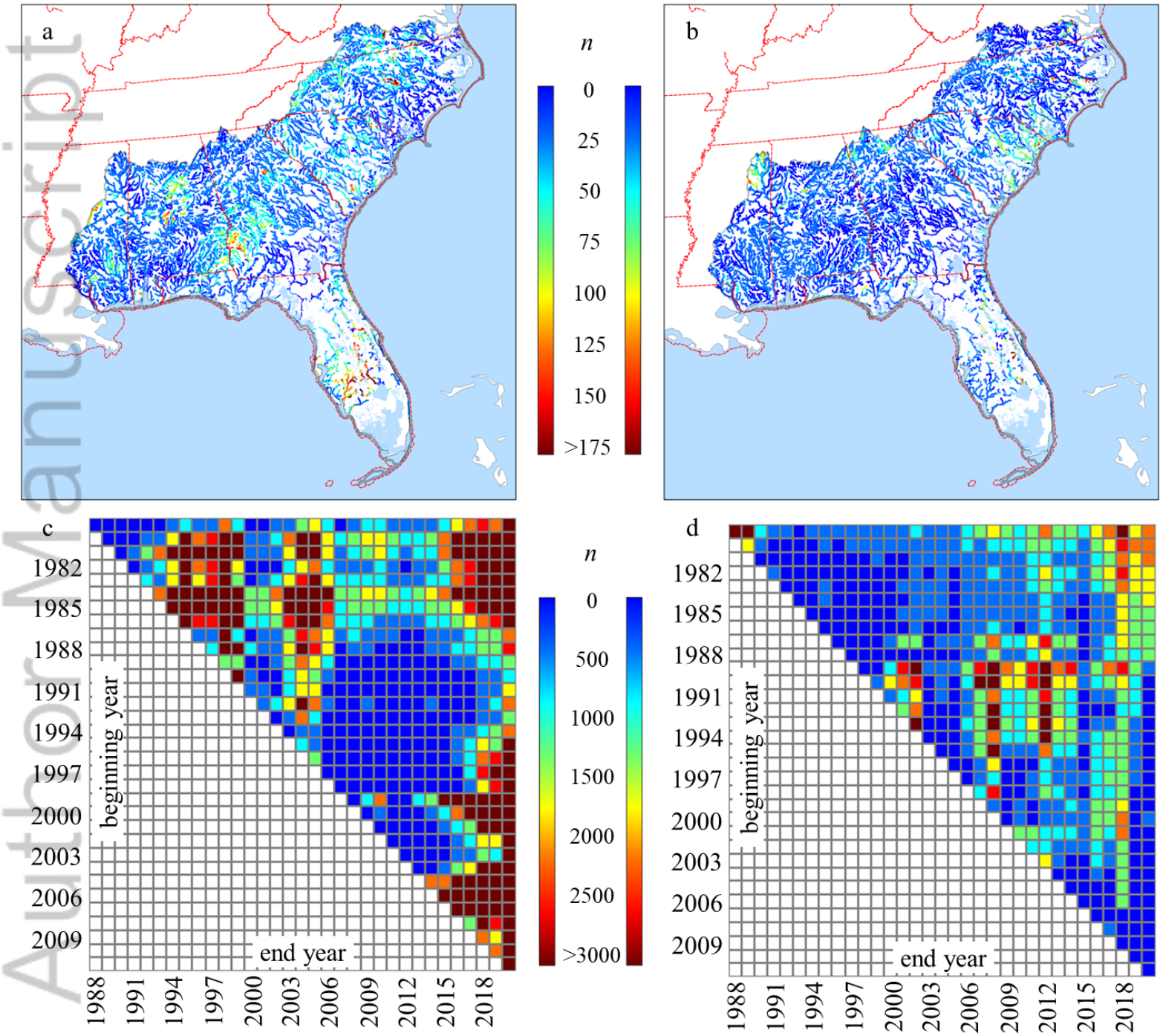

fig13.tif

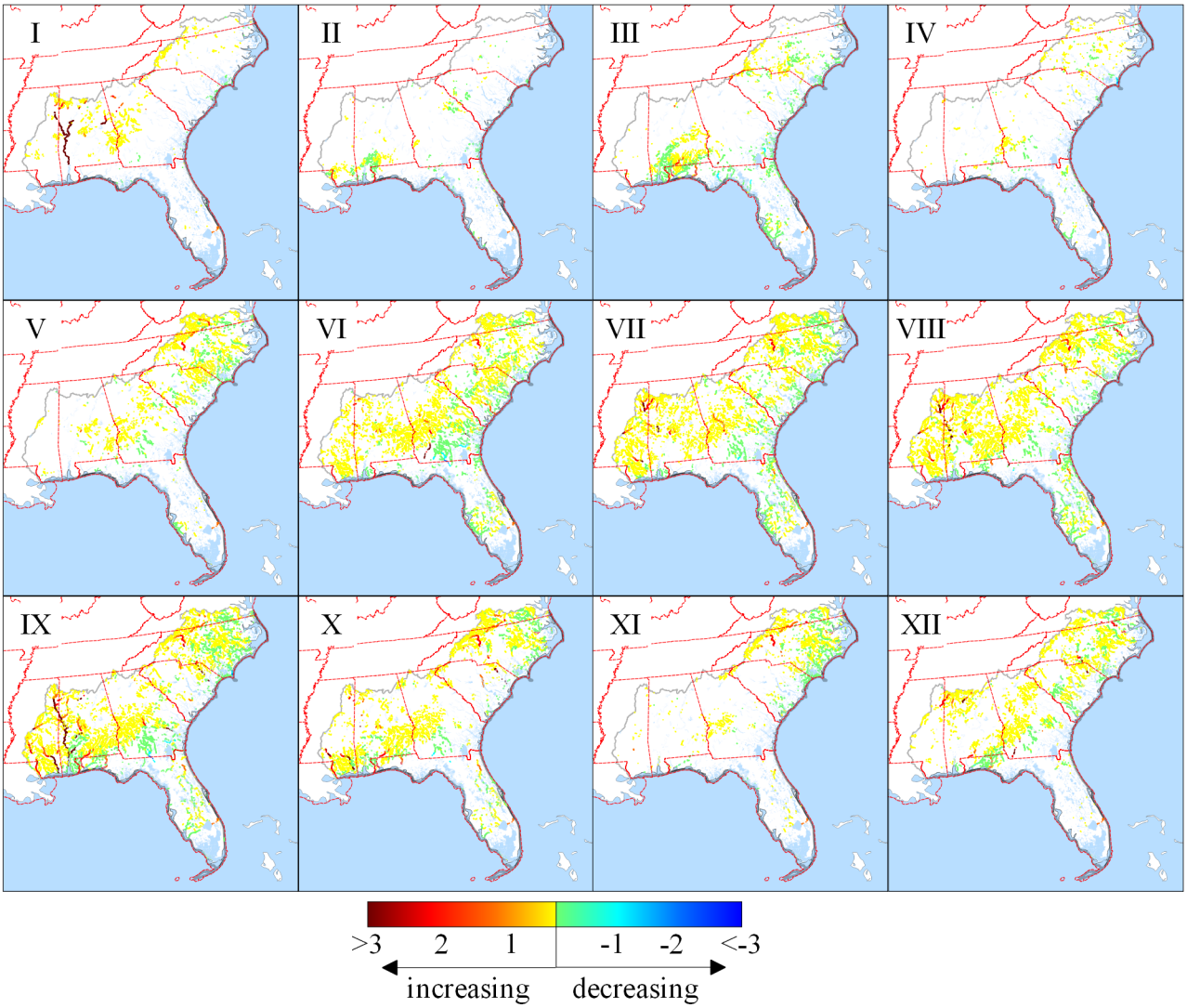

fig14.tiff

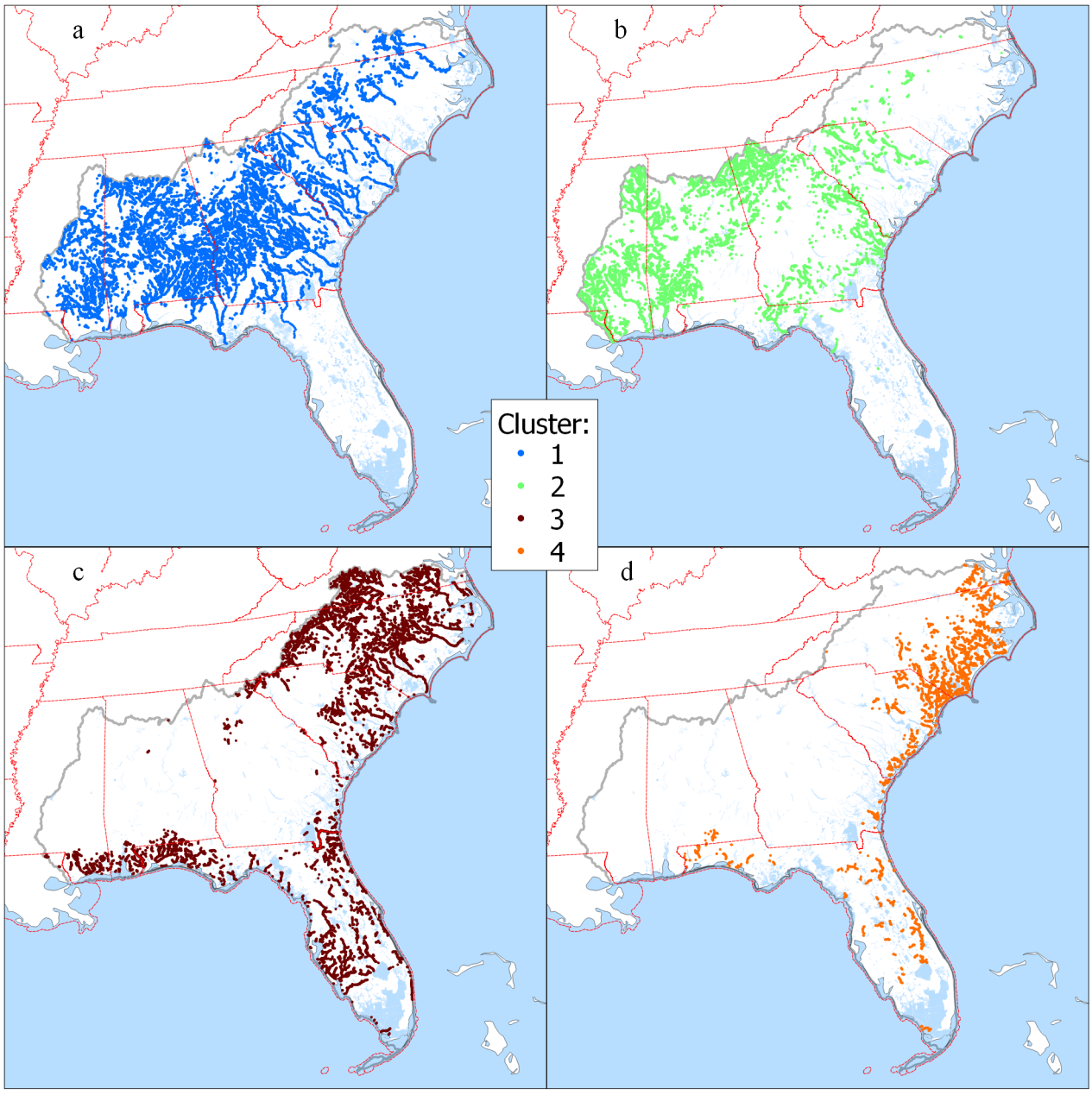

fig15.tiff

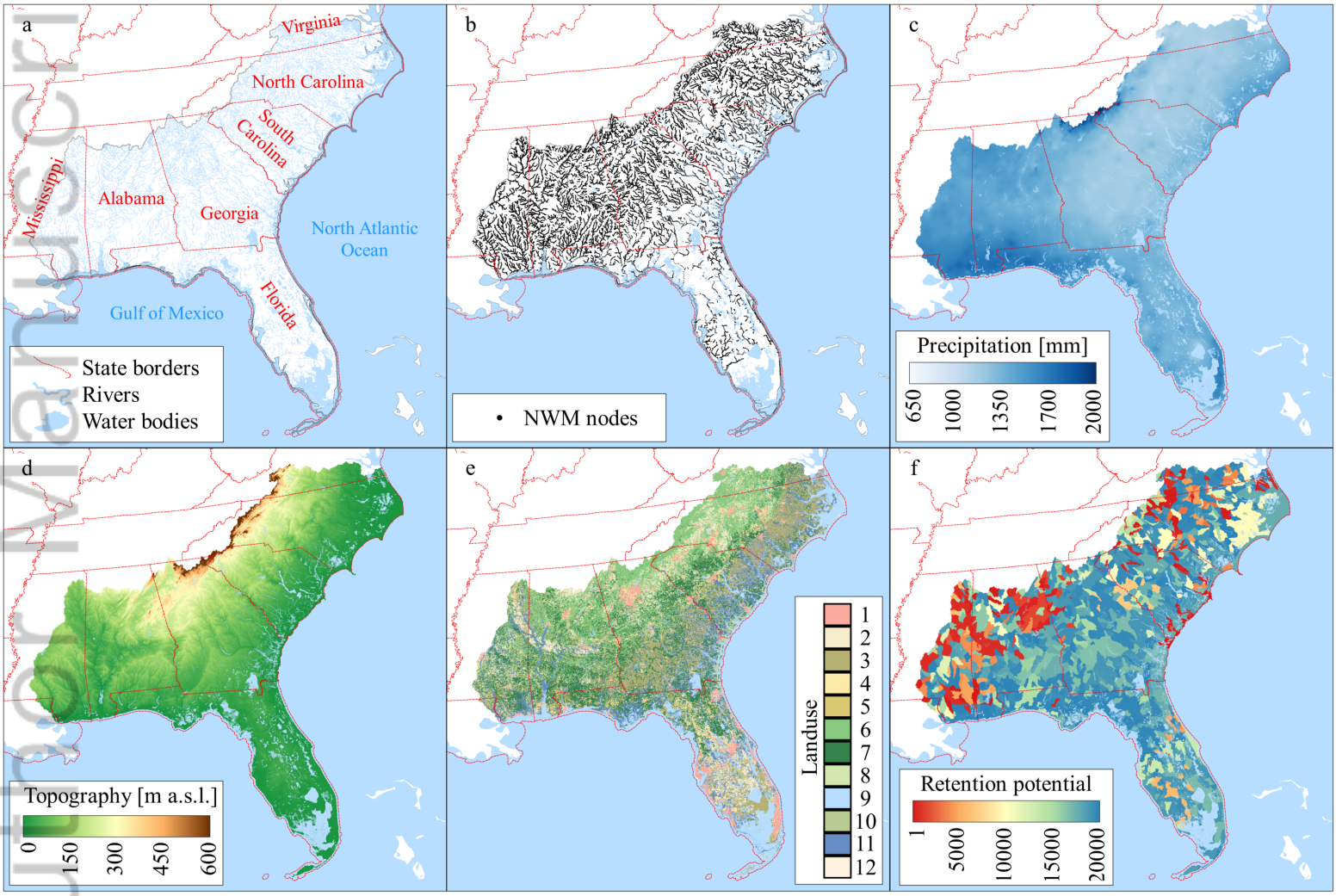

flood_fig1_alt600.tiff

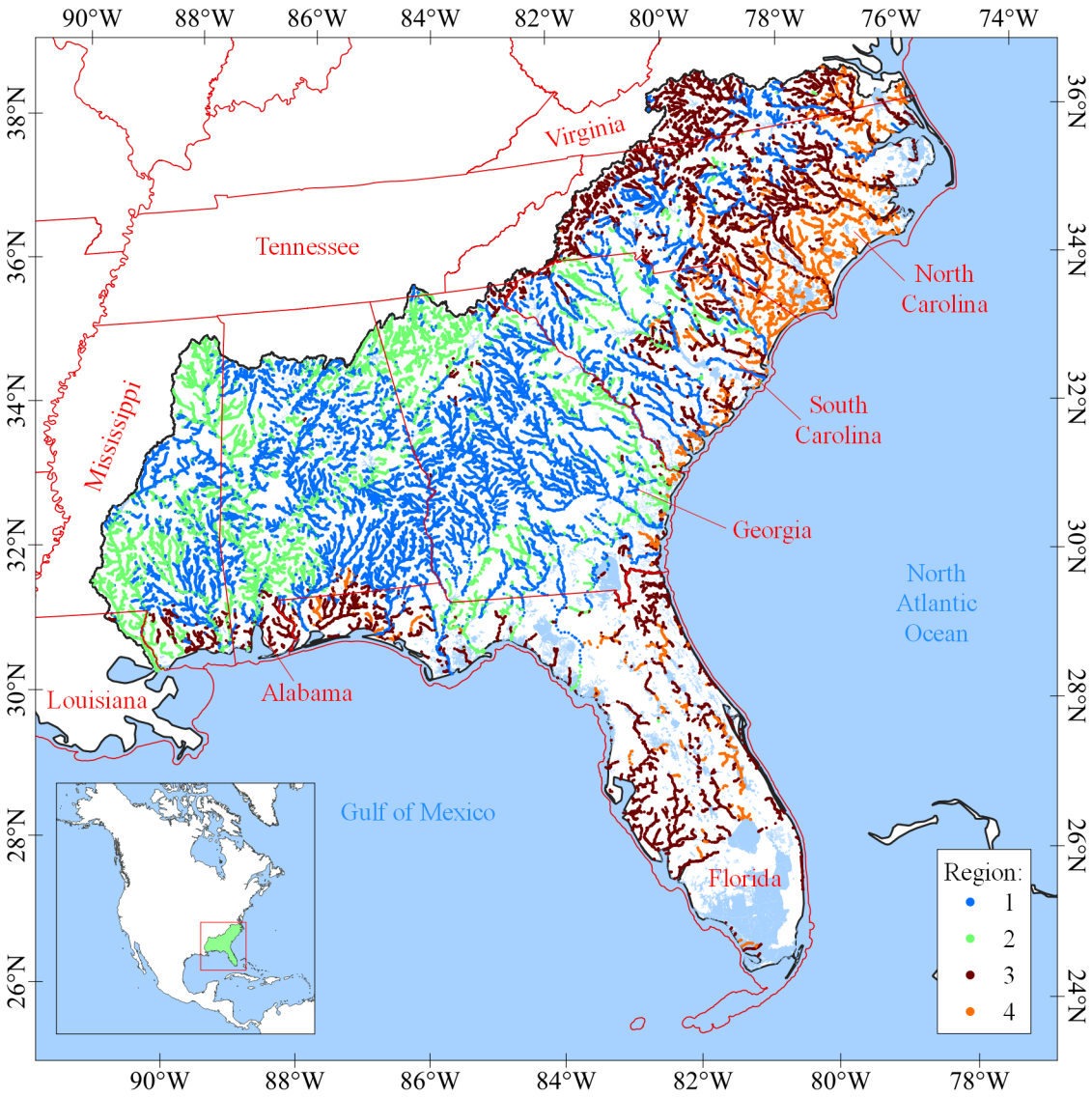

review1_ga.tiff

Central parts of Mississippi to South Carolina: high multiannual SFP occurrence with long total durations, high contribution to total discharge, and throughout the year occurrence with February and March peak.

South and north parts of Mississippi to South Carolina: similar parameters with increased flash flooding potential.

Florida, Gulf Coast, and parts of North Carolina and Virginia: lower occurrence and share in total discharge, with two peaks of occurrence in September-October and March.

Atlantic coast and parts of the Gulf coasts: lowest occurrence and shortest durations, with strong seasonal occurrence.